SPICAV: Spectroscopy for the Investigation of the Characteristics of the Atmosphere of Venus

Jean-Loup Bertaux[1], D. Nevejans[2], O. Korablev[3], E. Villard[1], J.P. Dubois[1], E. Neefs[2], E. Quémerais[1], F. Montmessin[1], F. Leblanc[1], E. Chassefière[1], E. Dimarellis[1], A. Hauchecorne[1], F. Lefèvre[1], P. Rannou[1], M. Cabane[1], G. Cernogora[1], G. Souchon[1], F. Semelin[1], M. Leclère[1], A. Reberac[1], C. Taulemesse[1], E. Van Ransbeek[2], S. Berkenbosch[2], R. Clairquin[2], C. Muller[2], F. Forget[4], F. Hourdin[4], O. Talagrand[4], A. Rodin[3], A. Fedorova[3], A. Stepanov[3], I. Vinogradov[3], A. Kiselev[3], Yu. Kalinnikov[3], G. Durry[7], B. Sandel[5] & A. Stern[6]

[1]*Service d'Aéronomie du CNRS, F-91371, Verrières-le-Buisson, France*
Email: jean-loup-bertaux@aerov.jussieu.fr
[2]*Belgian Institute for Space Aeronomy, 3 av. Circulaire, B-1180 Brussels, Belgium*
[3]*Space Research Institute (IKI), 84/32 Profsoyuznaya, 117810 Moscow, Russia*
[4]*Laboratoire de Météorologie Dynamique, 4 place Jussieu, F-75252 Paris Cedex 05, Paris, France*
[5]*Lunar & Planetary Laboratory, 901 Gould Simpson Building, Univ. of Arizona, Tucson, AZ 85721, USA*
[6]*SouthWest Research Institute, Geophysics, Astrophysics & Planetary Science, 1050 Walnut Ave., Suite 400, Boulder, CO 80302-5143, USA*
[7]*Groupe de Spectrométrie Moléculaire et Atmosphérique, Université de Reims Champagne-Ardennes B.P.1039, F-51687 Reims Cedex, France*

SPICAV (SPectroscopy for the Investigation of the Characteristics of the Atmosphere of Venus) is a suite of three UV-IR spectrometers dedicated to the study of the atmosphere of Venus, from ground level to the outermost hydrogen corona at more than 40 000 km altitude. It is derived from the SPICAM instrument already flying on Mars Express with great success, with the addition of the new Solar Occultation IR (SOIR) high-resolution spectrometer working in the solar occultation mode. In nadir orientation, SPICAV UV will analyse the albedo spectrum to retrieve SO_2 and the distribution of the UV-blue absorber (of unknown origin) on the dayside with implications for cloud structure, and atmospheric dynamics. On the nightside, the γ and δ bands of NO will be studied, as well as emissions produced by electron precipitations. In the stellar occultation mode, the UV sensor will measure the vertical profiles of CO_2, temperature, SO_2, SO, clouds and aerosols. The density/temperature profiles obtained with SPICAV will constrain and aid in the development of dynamical atmospheric models, from cloud top (~60 km) to 160 km in the atmosphere. UV observations of the upper atmosphere will allow studies of the ionosphere through the emissions of CO, CO^+ and CO_2^+, and its direct interaction with the solar wind. It will study the H corona, with its two different scale heights, and it will allow a better understanding of escape mechanisms and estimates of their magnitude, crucial for insight into the long-term evolution of the atmosphere. SPICAV VIS-IR uses pioneering technology: an acousto-optical tunable filter (AOTF). On the nightside, it will study the thermal emission peeping through the clouds, complementing the observations of both VIRTIS and PFS. In solar occultation mode, this channel will study the vertical structure of H_2O, CO_2 and aerosols. SOIR combines an echelle grating and an AOTF crystal to sort out one order at a time. The main objective is to measure HDO and H_2O in solar occultation, in order to characterise the escape of D atoms

from the upper atmosphere and give more insight into the evolution of water on Venus. It will also study isotopes of CO_2 and minor species, and provide a sensitive search for new species in the upper atmosphere. It will attempt to measure the nightside emission, which would allow a sensitive measurement of HDO in the lower atmosphere, to be compared to the ratio in the upper atmosphere, and possibly discover new minor atmospheric constituents.

1. Introduction

When ESA released an Announcement of Opportunity for a new Flexible science mission, the SPICAM team on Mars Express joined the group of scientists who proposed a mission to Venus, with a spacecraft as identical as possible to Mars Express carrying on-the-shelf instruments or copies of existing instruments. This was the case for VIRTIS, flying on Rosetta. Its IR capabilities make it the most important instrument of Venus Express, because it 'sees' the thermal emission from the ground and lower atmosphere, which was discovered from terrestrial telescope observations and glimpsed by Galileo and Cassini during flybys, but never studied from a Venus orbiter.

A Flexible mission has to be of moderate cost and fast development, so it was natural for the SPICAM team to propose a reflight of the instrument. At the same time, Korablev and Bertaux were designing a new type of high-resolution spectrometer. In the solar occultation mode, it would provide unique information about the HDO and H_2O content of the upper atmosphere of Venus, crucial for understanding the history of water on the planet. Nevejans and his team at the Belgian Institute for Space Aeronomy obtained funding from the Belgian Federal Science Policy Office to design and manufacture the Solar Occultation IR (SOIR) spectrometer in collaboration with a Belgian industrial partner (OIP). SOIR became a part of SPICAV.

While SPICAM is a 4.7 kg UV-IR instrument, SOIR had to be stacked on top to produce a single mechanical standalone package, with a mass of 13.9 kg. This implied a redesign of SPICAM's mechanical structure. Fig. 1 shows the arrangement of SPICAV UV and IR in the Mars Express configuration. For Venus Express, the cover is replaced by stiff walls to support a second floor for mounting SOIR.

SPICAV is thus a suite of three different spectrometers (Table 1). The UV spectrometer was refurbished from the SPICAM spare Flight Model. The IR channel was substantially modified, so a completely new Qualification Model and two Flight Models were fabricated. In spite of numerous difficulties owing to a very tight schedule, the complete Flight Model of SOIR was completed and tested in early 2005, and mounted on the spacecraft in May 2005.

Also, because the Sun faces the optical instruments during some mission periods, two additional hardware items had to be developed very quickly: two optical baffles on the spacecraft's +Z face (the common boresight axis of all the optical instruments), and a mechanical shutter activated by a stepper motor. Completing SPICAV is a common Digital Processing Unit (DPU), which provides the electrical and data interface to the spacecraft.

As a precursor to SPICAV UV, the Pioneer Venus UV spectrometer monitored the top of Venus' clouds and mesospheric airglow. With SPICAV UV, which registers all wavelengths at once, the signal-to-noise (S/N) ratio is much greater: >100 for each nm for 1 s integration. SPICAV UV is the first instrument at Venus to use the solar/stellar occultation technique that has proved to be very effective in studying the atmospheres of Earth, Mars and the outer planets.

Observations during the 18th century showed that light from the star Spica decreased abruptly during occultations by the Moon. It was concluded that the Moon has no atmosphere because, otherwise, refraction would have produced a

Table 1. SPICAV Principal Characteristics

Spectral bands	UV: 0.55 nm/pix; IR: 0.8 nm/pix at 1.5 μm; SOIR: 0.32 cm^{-1} at 2.4 μm
Spectral sampling	UV: 0.55 nm/pix; IR: 0.8 nm/pix at 1.5 μm SOIR: 0.32 cm^{-1} at 2.4 μm; 0.15 cm^{-1} at 4.0 μm
Mass	DPU+harness 0.865 kg; SU 13.05 kg; Total 13.915 kg; Sun baffles 0.47 kg
Power	DPU+SU 17.6 W, 26.4 W, 51.4 W
Volume	DPU: 161 x 142 x 70 mm; SU: 504 x 400 x 350 mm
Data rate	9, 34, 66 kbit/s
Data volume	Typical 100–400 Mbits / day
Observations	One onboard time telecommand, one SPICAV telecommand
Duration	Typically 5–30 min
Pointing (orientation)	Inertial star (also used for limb viewing); Inertial Sun; nadir

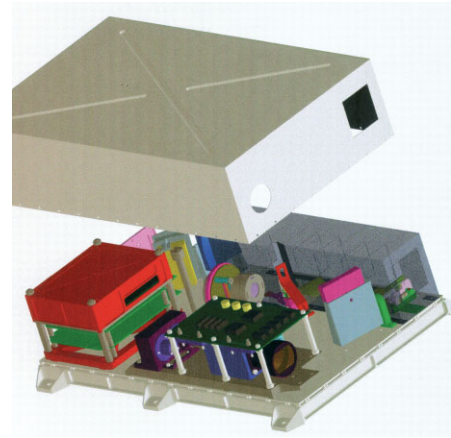

Fig. 1. Layout of the UV and IR channels. The IR AOTF spectrometer is at front left; the UV spectrometer is at the back. The common optical axis points to the right (+Z spacecraft axis).

progressive dimming of the star. The SPICAM/SPICAV acronyms are tributes to this early use of stellar occultation.

In the Earth's atmosphere, the occultation technique has been used to measure O_3 since the 1970s. Only one or two wavelengths were observed at a time in the early attempts, making identification of the absorber species uncertain. With the advent of multi-pixel detectors, the absorbing species can be safely identified by their spectral signatures. It also offers the potential to discover new, unexpected species in the atmosphere. The method of absorptive occultation spectroscopy is reviewed in Roscoe et al. (1994) and Smith & Hunten (1990). For terrestrial stratospheric research, it has become the most advanced method for long-term monitoring of ozone. In the IR, the most remarkable results are those of the ATMOS/Atlas Space Shuttle experiment, which provided a set of high-resolution IR spectra of the terrestrial atmosphere. In the UV-visible, NASA's SAGE-3 is using full-wavelength coverage of the Sun. Onboard Envisat, SCIAMACHY (Scanning Imaging Absorption Spectrometer for Atmospheric Chartography) is performing solar occultation and nadir observations, and the GOMOS (Global Ozone Monitoring by Occultations of Stars) instrument is dedicated to the monitoring of ozone and other species by stellar occultations (about 100 000 per year). SPICAV's methodology is clearly in line with the most advanced instrumentation for studying Earth's atmosphere.

With Venus Express, the three terrestrial planets each have a stellar-occultation instrument in operation, with GOMOS on Envisat completing the trio.

SOIR was proposed as a lightweight high-resolution solar occultation instrument to study the composition and structure of the atmosphere above the clouds. The typical resolution is ~0.2 cm^{-1} (resolving power 15 000–20 000) within a mass budget of < 6 kg and no moving parts. An echelle spectrometer is combined with an AOTF to separate the diffraction orders; the principle and the early prototypes were described by Korablev et al. (2002a; 2004). For planetary atmospheres, this approach offers a dramatic (an order of magnitude) increase in resolving power.

2.1 UV spectrometer description

A summary of the characteristics of the UV spectrometer is given in Table 2. It is almost identical to the UV channel on Mars Express. For better efficiency in

2. UV Observations

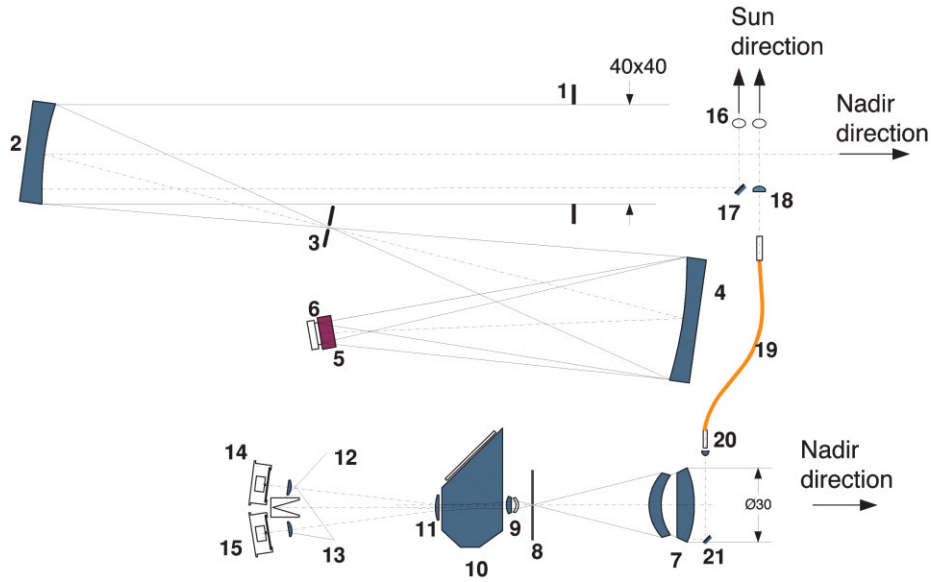

Fig. 2. Optical scheme of the UV and IR channels. 1: aperture of the UV channel; 2: off-axis parabolic mirror; 3: slit (can be changed from wide to narrow by a mechanical actuator, see text); 4: concave UV grating; 5: intensifier; 6: CCD; 7: IR channel objective; 8: IR FOV diaphragm; 9/11: collimating lenses; 10: AOTF crystal; 12: light trap for undiffracted light; 13: detector proximity lenses; 14: 'extraordinary' beam detector; 15: 'ordinary' beam detector; 16: solar opening (closed by shutter when not looking towards Sun); 17/21: flat mirror; 18: IR solar entry; 19: optical fibre; 20: fibre collimator.

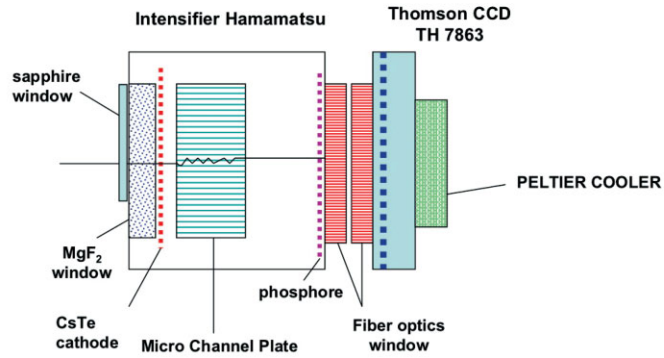

Fig. 3. The UV detector combines an image intensifier from Hamamatsu, transforming each UV photon at the entrance into a pulse of green light generated by the phosphor. The image is conveyed through two blocks of fibre optics, one included in the Hamamatsu detector, the other attached to the Thomson CCD.

the UV, it employs only two reflective surfaces (Fig. 2). The light flux is collected by an off-axis parabolic mirror, which reflects it into the entrance of the spectrometer. At the focal plane, a mechanical slit system has two modes: stellar occultations using no slit, and extended source observations with a slit. The slit defines the field of view (FOV), and is the entrance slit of the spectrometer. It is divided into two parts with different widths, allowing two spectral resolutions when observing an extended source. The first part (50 μm) gives good resolution with lower flux; the second (500 μm) gives more sensitivity at the expense of a coarser spectral resolution. The slit can be completely retracted, creating a hole corresponding to the total useful FOV of 2x3.16°. This configuration is used in the stellar occultation mode at dark limb when the spectrum of the star is recorded on a few lines of the CCD. The required pointing accuracy is 0.2°, but is so much better in practice on Mars Express that it has been possible to perform stellar occultations within the narrow part of the slit (0.02° wide).

A holographic concave toroidal grating from Jobin-Yvon, ion-etched to improve efficiency, feeds the detection block, with the dispersion direction perpendicular to the slit. Therefore, each point of the slit (or the focal plane, when there is no slit) has its spectrum formed perpendicular to the slit, on the photocathode of an image intensifier (Hamamatsu) with a CsTe cathode (UV-sensitive, but blind to visible light and $\lambda > 320$ nm), microchannel plate electron multiplier, and a phosphor output screen. The image ratio is ~1, which means

Table 2. Characteristics of the SPICAV UV

Primary mirror	Off-axis parabola 40x40 mm, coated MgF_2, f = 120 mm
Slit	50 µm x 4.6 mm; 500 µm x 2.2 mm
FOV	of a pixel 0.7x0.7 arcmin 2x3.16° no slit (stellar occultation) 0.24x0.95° with double slit
Spectral range	118–320 nm
Grating	holographic, concave, toroidal coated MgF_2, 290 lines/mm, blazed 170 nm
Spectral resolution per pixel	0.52 nm; spectral resolution 1.5 nm
Resolving power (occultations)	602–200 stellar; small slit
Resolving power (extended source)	120-300 small slit,~20 large slit
Pointing accuracy	< 0.2°
Detector	CCD Thomson TH7863 TE cooled at 270K, useful 288x384 pixels, 23x23 µm
Intensifier	Hamamatsu 200M, solar blind CsTe photocathode, input window CaF_2 + MgF_2
Vertical resolution	< 1 km (occultations), ~10 km (limb)

that a monochromatic image in the entrance of the spectrometer is conserved in the plane of the detector. The green image from the phosphor (Fig. 3) is transferred by custom-made fibre optic coupling to a Thomson CCD (TH7863) with 288x384 useful pixels and a masked zone of equivalent size. The pixel size is 23x23 µm. The 288 lines of the CCD are oriented along the spectral direction, and each line records the spectrum of one point of the entrance slit, with 384 spectral elements. The focal length of the telescope is such that one CCD pixel covers a FOV of 0.01x0.01º.

The spectral resolution for a point source determined by aberrations is about 1.5 nm, and one pixel of CCD samples 0.54 nm. The CCD detector has a Peltier cooler to reduce its temperature and associated dark current. On Venus Express, there is an additional thermal drain for better cooling of the camera electronics. Via custom-made fibre optics, the CCD is coupled with the output window of the image intensifier (Hamamatsu, type 200M). The solar-blind CsTe photocathode of the Hamamatsu intensifier has zero quantum efficiency beyond 320 nm, and is deposited on the internal face of the input window, made of MgF_2 to reach down to the Lyman-alpha wavelength (a SPICAV goal). An additional CaF_2 filter was glued above the window and covers it in part, preventing the overlapping of diffraction orders and Lyman-alpha straylight on Mars Express. However, Mars results showed that this extra window could be removed, in part because the contribution of the second order in a holographic grating is very small.

The focal length of the telescope is such that one CCD pixel covers a FOV of 0.01x0.01º. The slit of the spectrometer has two parts: narrow (0.02º wide by 1.9º long), achieving a spectral resolution of 1.5 nm (about 3 CCD pixels); and wide (0.2º wide by 0.98º long), achieving a higher photometric sensitivity for extended sources (factor ~8), at the expense of a reduced spectral resolution (6 nm). In principle, SPICAV can record 288 spatially-resolved spectra along its 2.88º-long slit (i.e. each spatial element subtending 0.02x0.01º on the sky). However, in practice, only five spectra are transmitted for each 1 s measurement in order to save data volume transmission. These are usually a sum of N individual spectra,

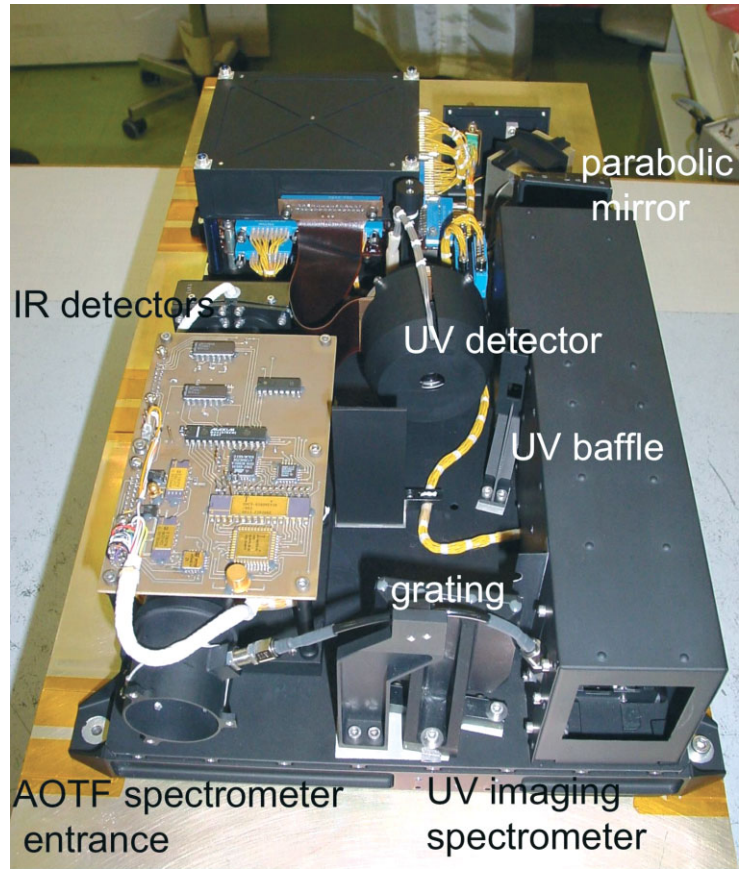

Fig. 4. First floor of SPICAV, with the UV and IR spectrometers side by side. The entrance of the UV spectrometer baffle is 5x5 cm.

with $N = 1, 2, 4, 8, 16$ or 32 CCD lines forming five adjacent spatial bins of variable extent (0.01–0.32°).

The gain of the microchannel plate (MCP) of the image intensifier may be adjusted by telecommand with a high voltage level from 500 V to 900 V, commanded by a digital level ('HT') from 0 to 255. When a photo-electron is created in the photocathode (a photo-event), it results in a pulse of light from the phosphor, distributed over a few pixels of the CCD. It is detected by the CCD reading electronics by a number of analogue-to-digital units (ADUs). At HT = 20 (a typical low gain to avoid saturation for dayside nadir observations), there are about two ADUs created per photo-event; for HT = 200, there 40 ADUs per photo-event The absolute calibration of the instrument is performed by numerous observations of hot UV stars and comparison with previous measurements by the International Ultraviolet Explorer (IUE).

There is a potential danger in activating the intensifier at a high gain on an intense source of light. High gain thus has to be used cautiously, on the dayside but at high altitude, and then on the nightside. One constraint of SPICAV operation is that during one observing period (ON-OFF), the parameters of the instrument may not be changed. In particular, when a fixed inertial attitude of the spacecraft is chosen, it must be certain that the signal will not damage the intensified detector if a high gain is used on a bright target.

Figure 4 is an overall view of the first floor of SPICAV FM1. SPICAV UV underwent a series of laboratory testings, some in full air but others in vacuum (wavelengths below 190 nm are absorbed by O_2 and H_2O). Fig. 5 is a full image of the detector when illuminated by a monochromatic light (Hg line emission at 253.7 nm). Image deformation by the optics means that each line of the CCD must be calibrated in wavelength. This is done (Fig. 6) by illuminating in vacuum

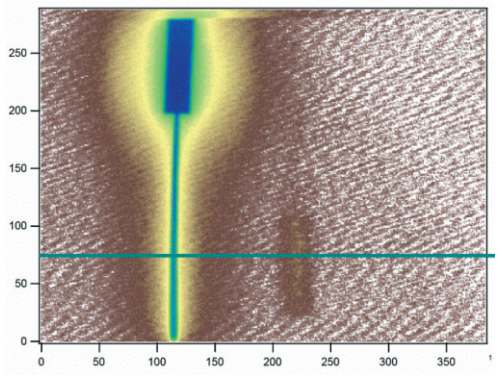

Fig. 5. The UV detector illuminated by monochromatic Hg line emission at 253.7 nm. The two parts of the slit are well seen. The curvature is due to image deformation by the optics, indicating a slight change in the wavelength calibration for each line of the CCD.

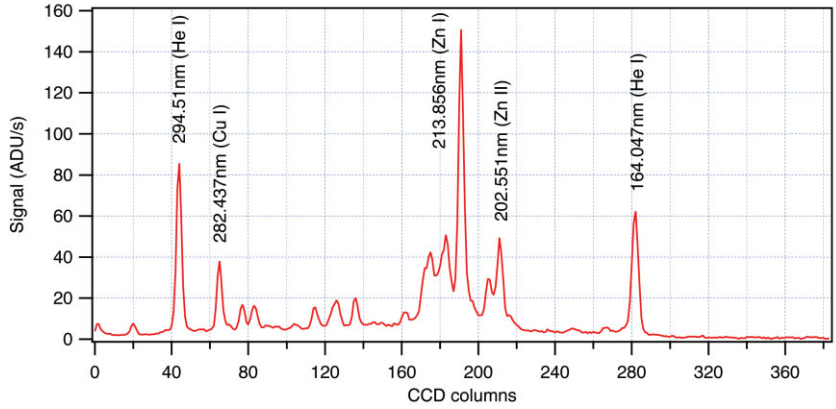

Fig. 6. The recorded spectrum of an HCl discharge lamp seen in vacuum by SPICAV UV for wavelength calibration. The wavelength extends from 110 nm at the right end to 310 nm at the left. There is no sign of second-order contamination (< 165 nm) in the first-order spectrum (> 220 nm).

the whole slit with a discharge lamp providing a number of known lines. In addition, numerous tests were performed in order to determine the overall sensitivity. The wavelength reflectivity of each component was tested under vacuum. The detector was calibrated by photon transfer, which yields the number of ADU generated in the CCD by a single photo-electron event, as a function of the high voltage applied to the MCP. The overall sensitivity is determined from the observation of hot stars with absolute flux known from Hubble Space Telescope and IUE observations (Bertaux et al., 2006). Good knowledge of the absolute sensitivity is necessary for quantitative analysis of emission measurements. It is not necessary for stellar/solar occultations: a ratio of spectra allows determination of the absolute quantity of absorbers.

2.2 Geometry of nightglow/dayglow limb observations: the tangential limb mode

Airglow spectroscopy and radiometry is a powerful method of investigation of the physics of upper atmospheres of the terrestrial planets. After the pioneering work of UV spectrometers aboard Mariner-6/7/9 (Barth et al., 1971; 1992), this technique was somewhat neglected for the following 30 years at Mars, except for rare observations in the extreme-UV with sounding rockets and Earth-orbiting observatories.

While dayglow was clearly measured and identified in the Mariner observations, the first detection of nightglow in the atmosphere of Mars was made with SPICAM (Bertaux et al., 2005). These successful observations are the result of the high sensitivity of SPICAM and the dedicated spacecraft operations to optimise the geometry of limb observations (Fig. 7), yielding higher signals than the Venus/Mars Express nominal nadir-looking geometry around pericentre.

The SPICAV UV FOV is boresighted with the other optical instruments

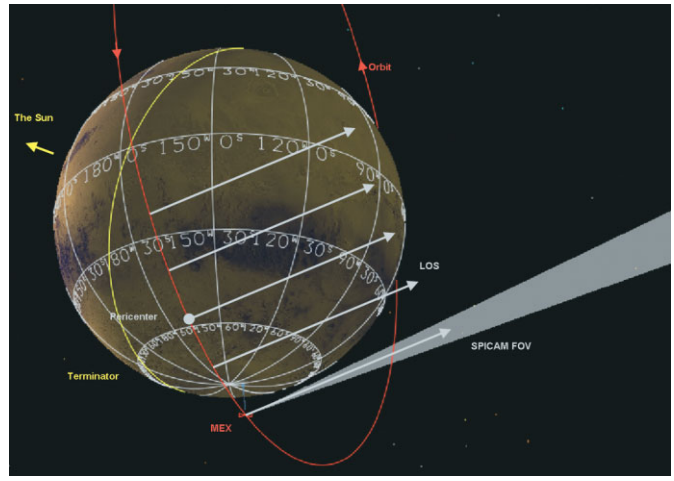

Fig. 7. The grazing-limb geometry maximises the time spent on observing the limb from an eccentric orbit, as used on Mars/Venus Express. The spacecraft is oriented with the +Z-axis (SPICAM line-of-sight) fixed inertially, scanning the limb twice. In this case, the line-of-sight was perpendicular to the velocity vector at pericentre, for optimum vertical resolution at the limb.

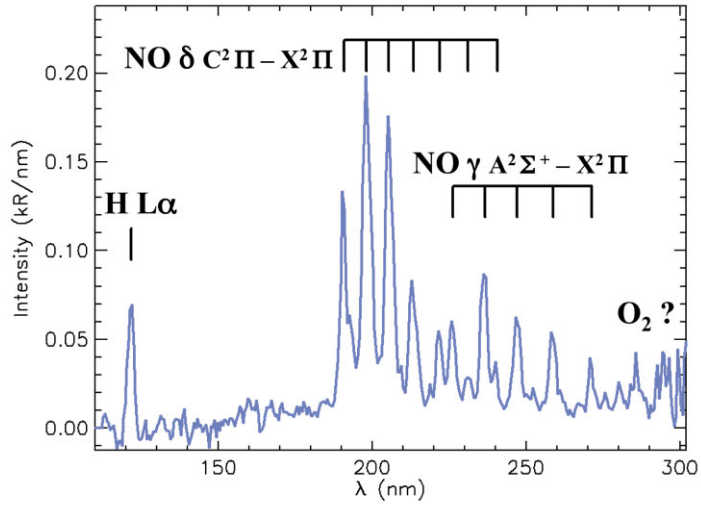

Fig. 8. Spectrum of the Martian nightglow obtained with SPICAM on orbit 734. Except for Lyman-alpha at 121.6 nm, all the observed lines coincide precisely with the main NO γ and δ vibrational state transitions responsible for the Venus NO nightglow. The absolute radiometric calibration comes from SPICAM observations of hot UV stars. The total NO intensity is 2.33 kR, with a 74% contribution of the δ-band (and 26% from γ-bands). The (0,1) line of the δ band alone is, at 475 R, 27% of the total δ bands. Spectral features above 280 nm could be attributed to the O_2 Herzberg I system, also expected from the recombination of O+O (taken from Bertaux et al., 2005).

(VMC, VIRTIS, PFS) and aligned with the +Z-axis of the spacecraft, usually maintained towards the nadir for imaging near pericentre. Another standard attitude is with the telemetry antenna (–Y) directed towards Earth. A third mode is when the spacecraft is maintained in a fixed inertial attitude, a mode heavily used by SPICAM for star occultation measurements, but also for limb observations. On the dayside, there are two reasons to look for limb emissions: to maximise the integrated emission (Chapman factor), and to eliminate the strong UV background of solar light scattered by the clouds at high altitudes (40–70 km).

Planning a limb observation requires finding an inertial direction such that, during the spacecraft's orbital motion, the line-of-sight (LOS) scans across the limb. In order to maximise the duration of the observation, a special type of observation was designed in which the LOS does not vertically cross the limb, but rather skims it tangentially, with a selectable minimum altitude (the 'tangential limb mode'). Geometry shows that, for any point M on the eccentric orbit, there are two LOS directions that skim the limb tangentially, with a specified minimum altitude Z_{min}. They are contained in the two planes tangent to the sphere $R_{Venus}+Z_{min}$ which also contain the tangent to the orbit at M (the velocity vector). One of them is selected to plan the observation, as well as M, according to the desired position of the tangent point at minimum altitude. One particularity of this kind of observation is that several geometrical parameters of

the LOS tangent point vary significantly and simultaneously during the observation (altitude, latitude, solar zenith angle).

Given the success of this mode of observation on Mars Express (two discoveries: NO bands at night and aurora), it will be used as much as possible on Venus Express.

2.3 The NO bands emission on the nightside

One conspicuous Venus nightglow emission is the γ and δ bands of nitric oxide (NO, 190–270 nm, respectively transitions $A^2\Sigma^+$-$X^2\Pi$ and $C^2\Pi$-$X^2\Pi$) produced when N and O atoms combine to produce the NO molecule. This UV emission was first observed with Mariner-5 (Barth et al. 1968) and later with Pioneer Venus (Stewart et al., 1979) in the night airglow of Venus, and identified (Feldman et al., 1979; Stewart & Barth, 1979) as NO radiative recombination. It was proposed that N and O atoms are produced by extreme-UV photo-dissociation of O_2, CO_2 and N_2 in the dayside upper atmosphere, and transported to the nightside where recombination occurs, a mechanism later supported by 3-D modelling (Bougher et al., 1990) and discussed thoroughly in terms of atmospheric circulation. There are no seasons on Venus, and the upper atmosphere at top cloud level (65 km) rotates faster than the solid body (super-rotation), with a period of 4–5 days. The subsolar point is a region of upwelling, and the circulation of the thermosphere is a combination of both the rotation, and a general motion from subsolar to antisolar point, axi-symmetric. Indeed, a maximum emission of NO night glow is found typically at local time 02:00, displaced from the anti-solar point by super-rotation, with an intensity of 1.9±0.6 kR, peaking at an altitude of 111±7 km (Stewart et al., 1980).

SPICAM detected for the first time the same type of NO emission on the nightside of Mars (Bertaux et al., 2005). Indeed, it is the major component of UV nightglow on Mars, together with H Lyman-alpha emission (121.6 nm). Fig. 8 shows the spectrum recorded in the Mars nightglow. The intensity is greater at Venus, offering a powerful diagnostic tool to compare with models of general circulation of the atmosphere-thermosphere system. Of particular interest are: the vertical distribution of the emission, which requires limb observations, and the latitude-local time distribution, which can be reached by nadir viewing, or during VIRTIS mappings of the nightside of Venus. It will allow the relative importance of the two systems of circulation to be disentangled: the super-rotation and the solar-antisolar circulation patterns.

2.4 Auroral emissions on Venus

Auroral emissions in planetary atmospheres 'are those that result from the impact of particles other than photoelectrons' (Fox, 1986). It is not only when energetic particles precipitate along magnetic field lines, as is the case at Earth and all the giant planets. Auroral activity has also been found on Venus, which has no magnetic field. On the Venus nightside, atomic O emissions at 130.4 nm and 135.6 nm appear in bright patches of varying sizes and intensities (Philips et al., 1986), which are believed to be produced by electrons with energies < 300 eV (Fox et al., 1991). This is a manifestation of the interaction of the atmosphere with the solar wind; this erosion of the atmosphere needs to be quantified to understand its evolution.

The potential of SPICAV to monitor these precipitations is illustrated by the first observation of an aurora in the Martian atmosphere, discovered by SPICAM (Bertaux et al., 2005). It is a new type of aurora not seen before in the Solar System. It is unlike auroras on Earth and the giant planets, which lie at the foot of the intrinsic magnetic field lines near the magnetic poles, and unlike the aurora at Venus, which is diffuse, sometimes spreading over the entire disc. Instead, the Martian aurora is a highly concentrated and localised emission controlled by the crustal magnetic field anomalies.

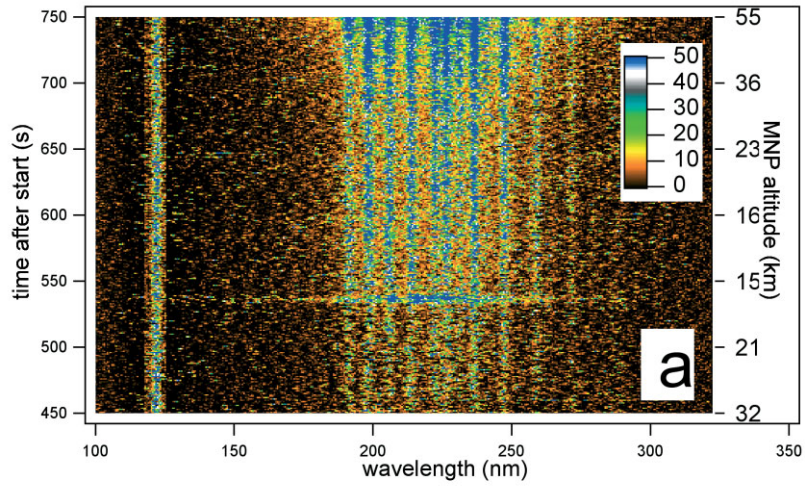

Fig. 9. Time variation of the Martian nightglow intensity spectrum recorded during a grazing-limb observation with spatial bin 2 (narrow slit, spectral resolution ~1.5 nm, one spectrum per second, data subset from 450 s to 750 s after the start of observation). It contains the H Lyman-alpha emission at 121.6 nm and a well-structured band (190–270 nm), identified as NO γ and δ bands (Fig. 8). The intensity in ADU/pixel is colour-coded. Altitudes of the Mars nearest point of the LOS are indicated at the right. At the time of the peak marked 'aurora' in Fig. 10, the spectra are obviously different from the typical NO spectrum.

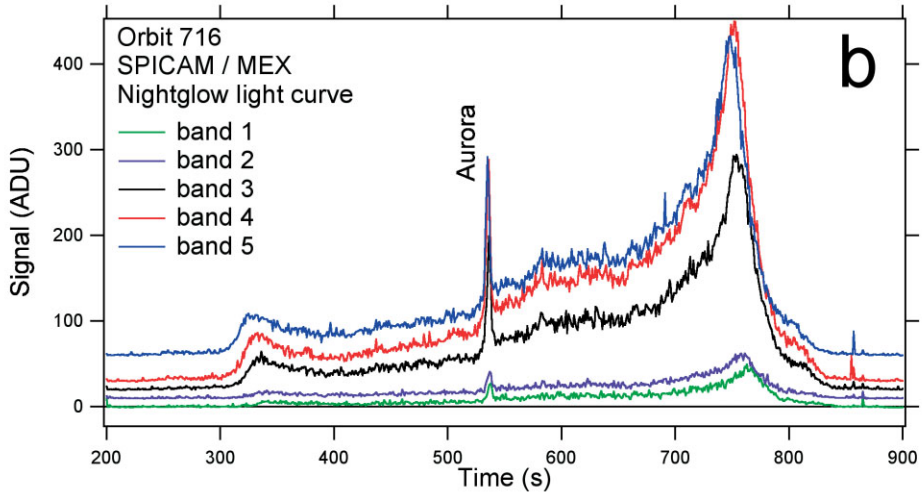

Fig. 10. Signal intensity for all five spatial bins as a function of time between 200 s and 900 s after the start of observations. Units are ADU per spectral pixel = 0.54 nm, averaged from 181 nm to 298 nm. There are 40 ADU per detected photon for the particular high voltage used here. The curves for spatial bins 2, 3, 4, 5 are vertically displaced for clarity (respectively by 10, 20, 30, 60 ADU). Spatial bins 3, 4 and 5 have low resolution but high sensitivity, and bins 1 and 2 are less sensitive but have higher spectral resolution. A conspicuous spike marked 'Aurora' is observed in all bins at time 535 s. This is the time at which the spectra in Fig. 10 differ from the usual NO spectrum. (From Bertaux et al., 2005).

please check figs 9/10/11 carefully and the text relating to them. The manuscript was confusing.

In the observation quoted here, the SPICAM LOS was permitted to drift slowly across the nightside limb to search for any weak emission, as sketched in Fig. 6. Fig. 9 is a colour-coded image of the time series of high-resolution intensity spectra. The most obvious spectral features are the H Lyman-alpha emission at 121.6 nm, and the well-structured band in the region 190–270 nm of the NO molecule, emitted when O and N atoms recombine, after having been produced by solar EUV photo-dissociation of CO_2, O_2 and N_2 on the dayside and transported to the nightside (Fig. 8).

In Fig. 10 the nightglow signal integrated over the wavelength range of the NO bands (181–298 nm) is displayed as a function of time for the five spatial bins. The signal is more intense for spatial bins 3, 4 and 5 than for spatial bins 1 and 2 because the FOV is wider and the source is extended. All curves show the same behaviour, almost identical to the variation of the NO emission observed 6 days later on orbit 734, which is explained by the variation of the altitude and the latitude of the Mars nearpoint when the LOS scans across the NO emitting layer, confined to the altitude range 60–80 km, and more intense at high southern latitudes (around time 750 s). There is, however, also a strong peak in all spatial bins between times 533 and 540 (increase by a factor 3 to 4), with no equivalent during orbit 734. The emission could be located by 'triangulation', using the five simultaneous FOVs of SPICAV UV. It coincides precisely with the region of strongest crustal magnetic field reported by Mars Global Surveyor (Acuña et al.,

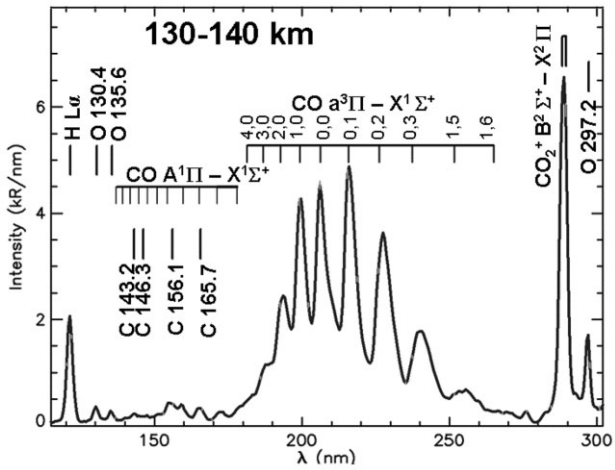

Fig. 11. Spectrum of dayglow recorded by SPICAM on the day side of the atmosphere of Mars (Leblanc et al., 2006).

2001); it indicates electrons moving along the magnetic field lines, possibly connected to the interplanetary magnetic field at this location and time. The detected horizontal extent of this aurora is 30 km minimum, but it could be more extended along the LOS. The altitude of the observed emission is 129±13 km. Still, it could extend more vertically, since it was scanned horizontally. The emissions in the auroral Mars spectrum (Fig. 10) are the CO $a^3\pi$-$X^1\Sigma^*$ Cameron band between 180 nm and 240 nm (694±50 R), long observed on the Martian dayside (Barth et al., 1971), as well as emissions associated with atomic carbon resonances and with the CO $A^1\pi$-$X\Sigma^*$ Fourth Positive Group between 135 nm and 170 nm, emissions associated with the CO_2^+ $B^2\Sigma^u$-$X^2\pi_g$ doublet at 289 nm (71±42 R). Lyman-alpha emission has been suppressed in Fig. 10 by subtracting spectrum a from spectrum b (which also indicates there was no increase in this emission during this time).

Auroras on the nightside of Venus are one sign of the interaction of the solar wind with the ionosphere and the neutral atmosphere. This interaction is a major player in the erosion of the atmosphere, participating in its evolution through escape, and isotopic differential escape. As such, it is important to measure the aurora to quantify this escape mechanism. The use of models such as TRANSCAR, adapted to Venus, are important in this respect.

2.5 Airglow observations at the limb

2.5.1 Study of the ionosphere from UV

The natural UV airglow of the atmosphere offers the possibility of remotely studying the ionosphere and its temporal behaviour as a function of solar-wind parameters. Fig. 11 shows the spectrum of dayglow recorded by SPICAM on the dayside of the atmosphere of Mars (Leblanc et al., 2006). Similar emissions have been observed on the dayside of Venus, as reported in Fox (1992). The main ionisable neutral constituent is CO_2, and the CO_2^+ transition ($B^2\Sigma^u$-$X^2\pi_g$) at 289 nm (or 2890 Å) is produced by photoionisation of CO_2 from solar UV at $\lambda < 69$ nm. The other band, CO_2^+ ($A^2\Sigma^u$-$X^2\pi_g$) between 300 nm and 400 nm, is produced by a combination of photoionisation and fluorescence scattering on CO_2^+ ions. The SPICAM UV long-wavelength cut-off is at 320 nm, which is enough to measure the (4,0) and 3,0) transitions of the A-X band.

The intense Cameron band of CO $a^3\pi$-$X^1\Sigma^+$ observed at 190–270 nm is produced by a combination of photo-dissociation of CO_2 by solar UV ($\lambda < 108$ nm), electron impact dissociation of CO_2, and dissociative recombination of CO_2^+. The variation of this band intensity with altitude was used to determine the vertical profile of CO_2 above 120 km, and from the scale

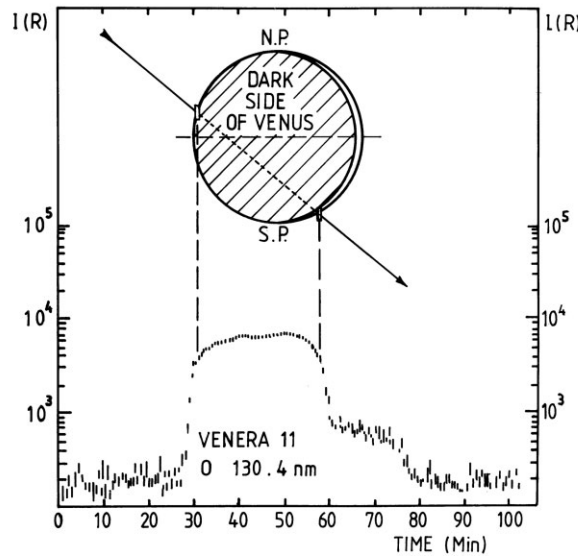

Fig. 12a. The hot corona of O at 130.4 nm, as seen from Venera-11 (Bertaux et al., 1981). The orbit passes behind the planet; the LOS is directed out of the page. The bulge of the hot corona is located at high latitudes in the afternoon side. It was not seen by Venera-12 flying by Venus 4 days before in a similar geometry. Note the puzzling two-slope behaviour of the intensity, not expected from models.

height the temperature of the thermosphere was derived in the atmosphere of Mars (Stewart et al., 1972). This indirect method of determining CO_2 could be validated with SPICAV UV, when a stellar occultation is performed on the dayside. If the Venus Express pointing is as good as at Mars, the small slit of the FOV will be used, and the bright stellar spectrum would show up, superimposed on the general airglow only on a few lines of the CCD. The analysis of the spectro-image would provide information on CO_2: direct measurement by absorptive occultation, and indirect CO Cameron band emission. Neutral O and neutral H vertical density profiles will be derived from the vertical variation of their resonance lines at 130.4 nm and 121.6 nm (Lyman-alpha), respectively.

2.5.2. Hot oxygen corona and hot hydrogen corona of Venus

The coronae of H and O atoms have been reviewed by Paxton & Anderson (1992). While $CO_2 + h\nu \rightarrow CO_2^+$ is the main photo-ionisation source, it is the O_2^+ ion that is the most abundant. As a result, a hot atomic oxygen corona was detected by Venera-11 (Bertaux et al., 1981) around Venus from the emission at 130.4 nm (Fig. 12a), and is an interesting target for Venus Express. This may be an important source of O escape from the atmosphere of Venus, somewhat equilibrating the escape of H atoms responsible for the measured enrichment of the D/H ratio (a factor of ~150) detected by the Pioneer Venus mass spectrometer (Donahue et al., 1982) and confirmed in the IR in the lower atmosphere.

The H corona of Venus is peculiar, since it displays a radial distribution with two scale heights, one corresponding to the normal exospheric temperature (~300K), and the other at ~600K (Fig. 12b), which dominates at larger distances (above ~4000 km altitude). The common explanation is that the 'hot' H population is produced by non-thermal reactions below the exobase (at ~300 km altitude). However, a detailed analysis of the H vertical profile obtained from Lyman-alpha measurements with the Venera-11 and -12 UV spectrometers (Bertaux et al., 1982) suggested that this population was absent below ~ 400 km (Fig. 12c), casting some doubt about the region of origin and actual mechanism of production of this hot H population. The detailed vertical profiles obtained at the limb with high vertical resolution (which requires limb observations near the pericentre) will clarify this puzzle, and help to quantify the present escape rate of H and O atoms by non-thermal mechanisms. The thermal (Jeans) escape is easy to compute, once the exobase density and the exospheric temperatures are determined by SPICAV UV from the vertical altitude distribution of H and O

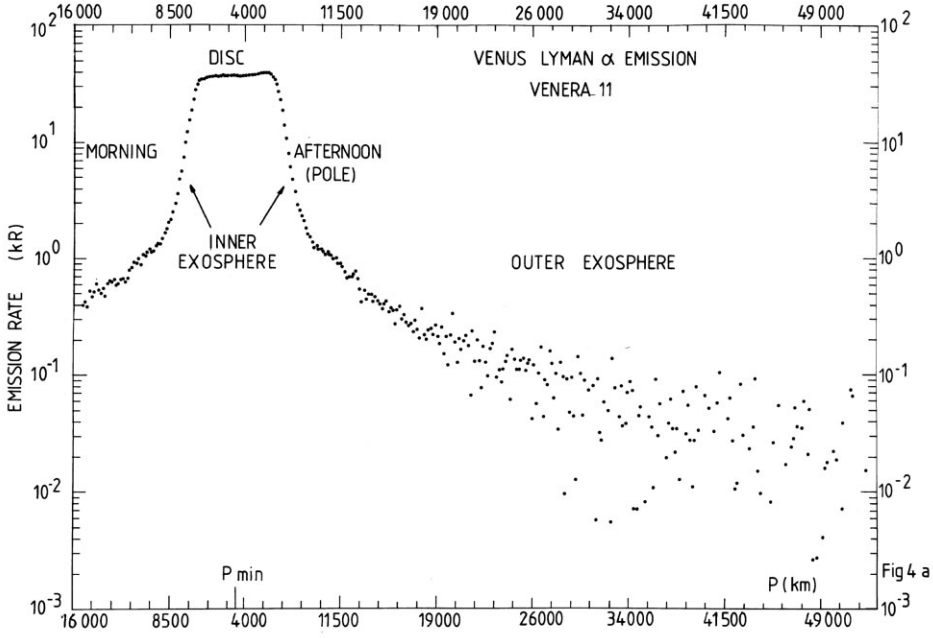

Fig. 12b. The hydrogen corona of H at Lyman-alpha 121.6 nm, from Venera-11 and -12 measurements, as a function of impact parameter of the LOS. The two different slopes are seen on both sides of the planet: cold component below 10 000 km (LOS distance to planet centre), hot component above 10 000 km. Note the shoulder at 10 000 km, not predicted by models (from Bertaux et al., 1982). It could be argued that the data suggest three scale heights, with a change of slope for the cold component at about 8000 km on the afternoon side.

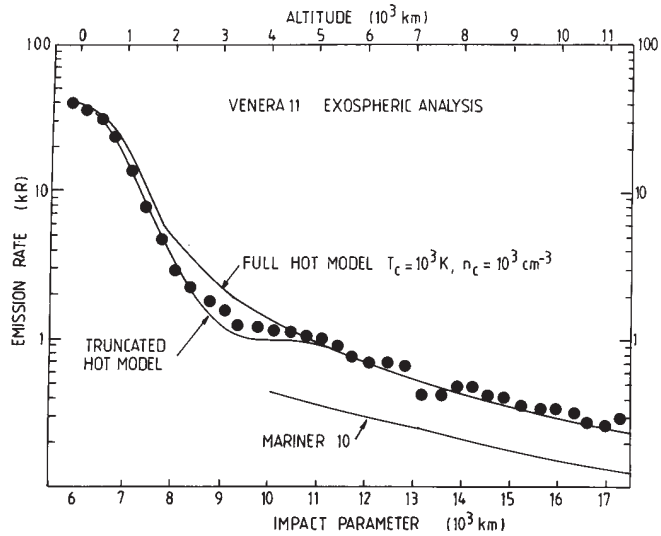

Fig. 12c. Close up of the H corona at Lyman-alpha 121.6 nm. The hot component measured by Venera-11 in 1978 is double the intensity measured by Mariner-10 in 1974, possibly owing to higher solar activity. Note the deficit of the hot component around 4000 km altitude (from Bertaux et al., 1982).

atoms. An essential tool for interpreting the H and O intensity data is a good radiative transfer model, such as the one developed at Service d'Aéronomie by Bertaux and maintained and improved by Quémerais and Chaufray.

2.5.3. Atmospheric escape and D/H ratio

At present there is only 3 cm of water in the atmosphere of Venus (if condensed into liquid form), in comparison with ~3 km on Earth. The current explanation is that water escaped from the upper atmosphere, because H atoms can escape. The D/H ratio is enriched by a factor of 150, compared to Earth (Donahue, 1999; Donahue et al., 1982; De Bergh et al., 1991). This is explained by isotopic differential escape: D atoms are twice the mass of H atoms, and so less prone to escape. Suppose that no D atoms could ever escape. The present content of D atoms would then reflect the total water that was in the atmosphere of Venus: 4.5 m, very small compared to Earth. Therefore, it is crucially important to

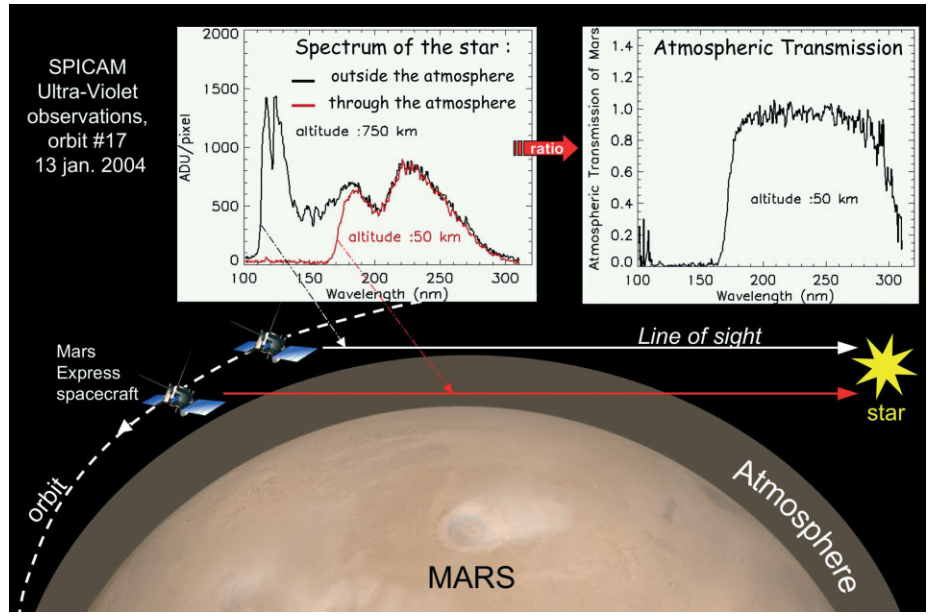

Fig. 13. Principle of stellar occultation measurements. From the two spectra obtained outside and through the atmosphere, atmospheric transmission can be derived as a function of wavelength. The spectra shown are from the very first stellar occultation made by SPICAM on Mars Express (it was also the very first made by any instrument orbiting Mars). Shortward of 180 nm, the signal is completely absorbed by CO_2. The situation for Venus Express is similar.

measure the quantity of D atoms and HDO in the upper atmosphere of Venus, to estimate the rate of escape of D atoms. HDO is addressed by the SOIR spectrometer (see below). For D atoms, the situation is unclear. Both D atoms and H atoms produce a Lyman-alpha resonant emission in the upper atmosphere, excited by the H solar Lyman-alpha line. Since the wavelength separation (H 121.566 nm; D 121.533 nm) is larger than the thermal width of each line, the radiative transfer of both types of Lyman-alpha are totally decoupled. If the D/H ratio in the upper atmosphere (>120 km where D and H atoms are illuminated by the Sun without CO_2 absorption) was similar to the lower atmosphere ratio of HDO/H_2O, then from outside we could see the emission of Lyman-alpha of D atoms, well separated from the H emission, at a level of more than 1 kR. However, Bertaux & Clarke (1989) used the IUE observatory and found no D emission at all, to a much lower limit than 1 kR. Therefore, there is possibly a mechanism that prevents D atoms from getting into the upper atmosphere. With Lyman-alpha measurements from the Hubble Space Telescope, Krasnopolsky et al. (1998) reported that the D/ H ratio in the upper atmosphere of Mars was lower by a factor of 10 than the D/H ratio in the lower atmosphere. A possible explanation (Cheng et al., 1999) is that HDO is less photo-dissociated than H_2O, because of its smaller cross-section. This effect is probably insufficient to explain the discrepancy, and another explanation has been shown to be also important (Bertaux & Montmessin, 2000): fractionation through condensation. HDO is more prone to condense in ice crystals than H_2O from the vapour phase, reducing the D/H ratio when altitude is increasing in regions where the photo-dissociation rate is important. This effect is known to play an important role in the Earth's upper troposphere-stratosphere, where HDO is severely depleted just above the tropopause. It is also likely to be operating at Mars. SPICAV will determine the situation on Venus, mainly with SOIR solar occultations measurements of HDO and H_2O simultaneously in the upper atmosphere.

Though SPICAV UV has insufficient spectral resolution to distinguish H and D Lyman-alpha emissions, they could be tentatively separated from the vertical distribution of the sum intensities. While the H emission should present a smooth variation around the CO_2 absorption limb (around 120 km), because it is optically thick, the D Lyman-alpha emission is optically thin, and the intensity

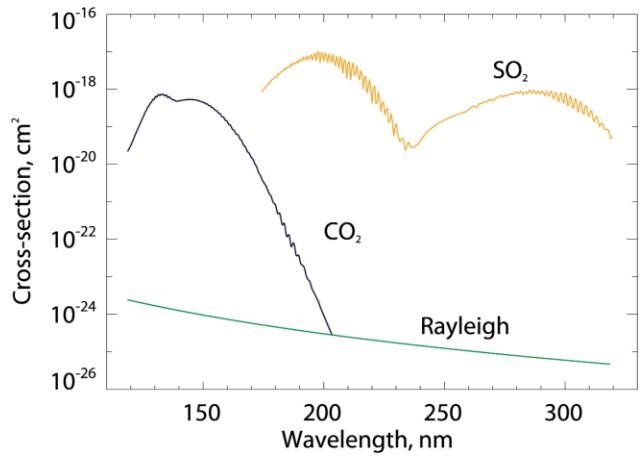

Fig. 14. Extinction cross-sections of CO_2 and SO_2, characteristic for the Venus atmosphere in the spectral range of SPICAV. The Rayleigh extinction of CO_2 is also displayed. Aerosols/dust would add to the absorption everywhere in wavelength with a slope characteristic of the size of particles.

doubles just above the limb. Any spike at the CO_2 limb in the vertical distribution of Lyman-alpha total intensity limb (estimated to be ~1 kR) would be due to D atoms. Therefore, both D and H abundances could be determined in the upper atmosphere, and compared to HDO/H_2O measurements in the lower atmosphere in the IR, and also at high altitude with SOIR.

2.6. Atmospheric vertical profiling by stellar occultation in UV

2.6.1 Overview of stellar occultations

In the stellar occultation mode, SPICAV UV will measure the vertical distribution of CO_2, temperature, SO_2, aerosols and possibly O_2. The principle is simple (Fig. 13). Along the orbit, stars are occulted one after the other by the planetary limb opposite to the velocity vector. At a predetermined time, the spacecraft is oriented for SPICAV UV to view a given star. The spectrum recorded above the atmosphere (say, at 200 km), unaltered by atmospheric absorption serves as a reference spectrum. Then, as Venus Express is maintained in a 3-axis inertial attitude, the line-of-sight to the star slices deeper and deeper into the atmosphere, down to total occultation.

The stellar occultation technique offers three decisive features:

— an absolute concentration derived from a relative measurement (self calibrated no need for instrument calibration);
— excellent vertical resolution, whatever the distance to the planet (because the star is a point source);
— knowledge of the accuracy of the measurement altitude, in contrast with limb-emission methods, is independent of the attitude of the spacecraft. The LOS is entirely determined by the direction of the star in the sky (known) and the position of the spacecraft on its orbit;
— stellar occultations are performed preferably on the nightside, to avoid contamination by the bright limb, and do not affect the operation of dayside mapping instruments. Several (3–5) occultations per orbit are planned, the limiting factor being the spacecraft orientation as a resource to be shared between the various investigations.

The orbit is fixed in inertial space; when a star is occulted on one orbit, the same star is occulted during the following orbits at the same latitude. Therefore, suitable stars must be found for occultations at various latitudes. The occultations are repetitive, unlike for Mars Express, which has a rapidly changing orbit. Hot stars are preferred, because they are brighter in UV. Their spectrum is flatter in UV than the solar spectrum. 'Deoccultation' (stellar rise) is

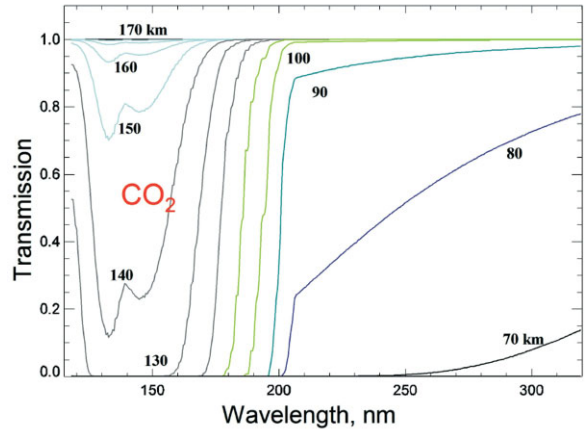

Fig. 15. Synthetic spectra of Venus atmosphere transmission in occultation for various grazing altitudes. SO_2 is not taken into account in this simulation.

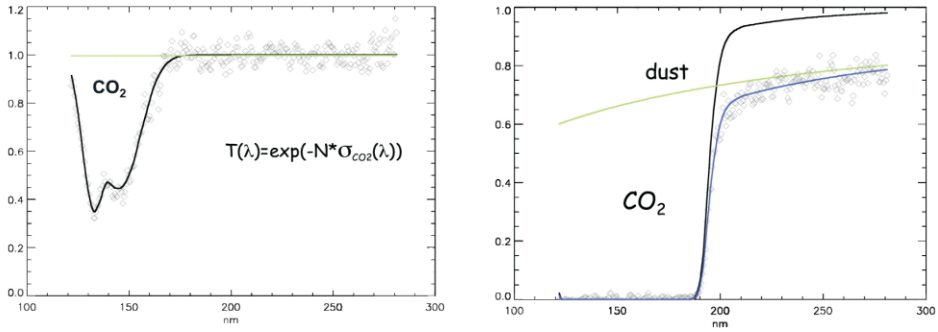

Fig. 16 (left). SPICAM measurements of spectral atmospheric transmission during one stellar occultation at high altitude, where only CO_2 absorption is present.

Fig. 17 (right). As Fig. 16, but lower in the atmosphere. The green curve is the absorption attributed to aerosols necessary to fit the data, in addition to CO_2 absorption and Rayleigh extinction.

also possible, since there is no closed-loop tracking system. There are many occultation opportunities around pericentre, because Venus is then much larger in the FOV and thus occulting more sky. Dedicated occultations will thus be requested near pericentre.

Figure 14 shows the absorption cross-sections of CO_2 and SO_2 in the UV as a function of wavelength. O_2 is absorbing (Schumann-Runge bands) near the long-wavelength edge of CO_2, providing the possibility of measuring O_2. Other absorbers are dust (Mie-scattering generalised to non-spherical particles), and SO_2. The atmospheric transmission simulations are presented in Fig. 15 for various tangential heights. Besides CO_2, an SO_2 and dust profile was assumed. Rayleigh extinction by CO_2 was included in the simulations. While on Mars, 30–40 km can be reached most of time, but the clouds on Venus will prevent anything below 60–70 km.

Because the CO_2 cross-section presents an enormous dynamic range in the UV, the CO_2 absorption may be already be detected at an altitude of 150 km. For decreasing tangential heights, the CO_2 manifests itself by a sharp cut-off that increases in wavelength, up to ~200 nm at 80 km altitude (Fig. 15). Longward of 200 nm, the transmission spectrum is dominated by SO_2, dust and CO_2 Rayleigh extinction. The Rayleigh extinction above 200 nm can be computed from the CO_2 line density determined below 200 nm, and the remaining continuous absorption above 200 nm may be attributed to dust/aerosol for a determination of its vertical distribution and spectral characteristics in the UV, as illustrated by SPICAM actual measurements (Fig. 16 and 17) for one stellar occultation at high altitude, where only CO_2 absorption is present.

Results of stellar occultations from Mars Express have been presented at a number of conferences; see Quémerais et al. (2006) on the actual data and inversion processes, Montmessin et al. (2006) for the cloud and dust distribu-

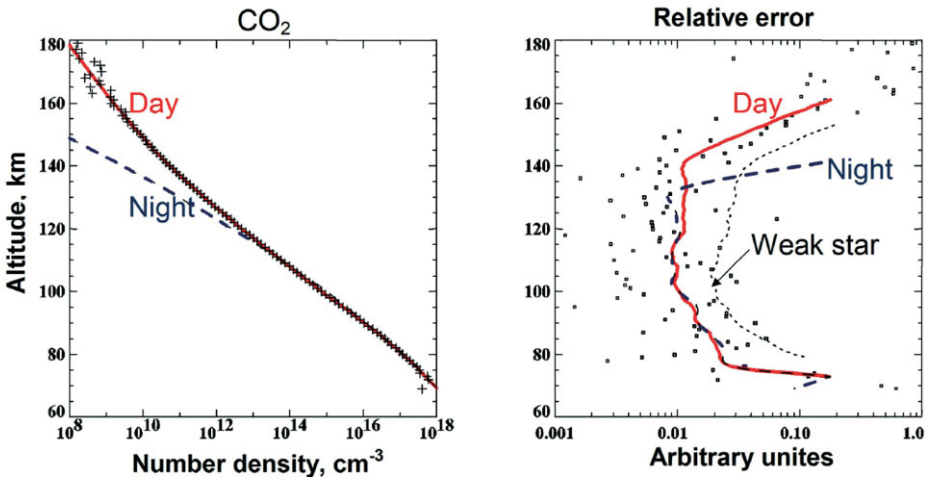

Fig. 18. Simulation of the retrieval of Venus atmospheric density in stellar occultation (Korablev & Bertaux, 2003). Note the large difference of density between the day and night sides. The temperature error is below 5–10% for most of the profile.

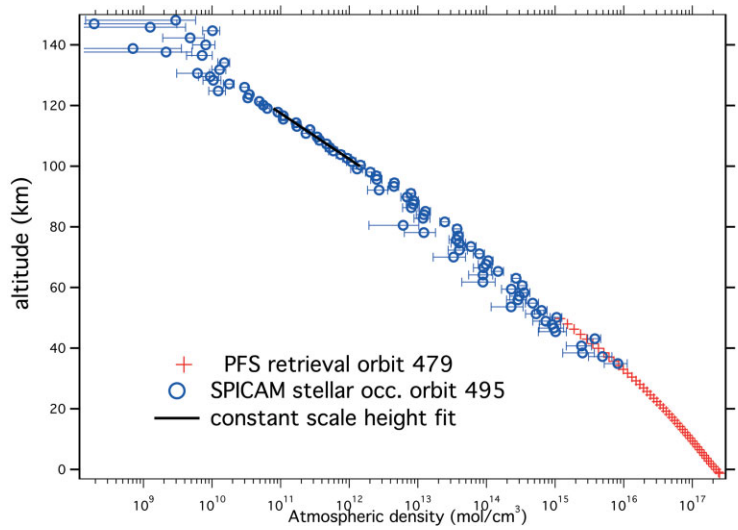

Fig. 19. An example of density retrieval in the atmosphere of Mars, with the PFS data also plotted (courtesy V. Formisano). It illustrates the good agreement between and the complementarity of the sets of measurements; the same applies for Venus.

tions, Forget et al. (2006) for discussion of the CO_2 density and temperature measurements, and Lebonnois et al. (2006) for the ozone results.

2.6.2 CO_2 density and temperature profile

Once the line density of CO_2 is determined from the transmission spectra for each altitude (one altitude per second), the local density $n(z)$ is determined from Abel's vertical inversion of the line density vertical distribution during a single occultation. Then, the hydrostatic equation allows temperature to be determined (Quémerais et al., 2006). Fig. 18 is a simulation of the retrieval of atmospheric density in stellar occultation (Korablev & Bertaux, 2003). Fig. 19 is an example of density retrieval in the atmosphere of Mars; PFS data are also plotted, illustrating the good agreement and the complementarity of both sets of measurements as a function of altitude.

There is a known dependence of CO_2 absorption cross-section on the temperature T; the retrieval process begins by a first iteration with an *a priori* profile $T(z)$ and corresponding choice of CO_2 cross section. Then, N **xxx what is N ?? xxx** and n are retrieved, and the scale height is derived, independently of a wrong choice of the cross-section, providing a new estimate for $T(z)$. A few iterations allow convergence. However, this has not yet been implemented for Mars Express in the SPICAM data reduction pipeline.

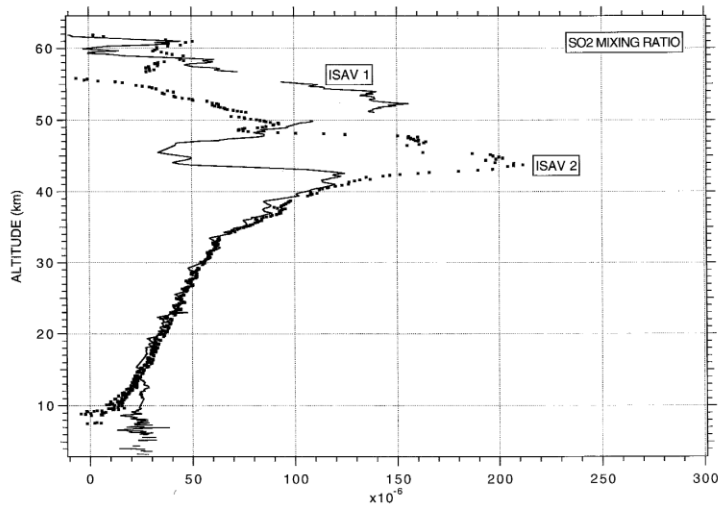

Fig. 20. ISAV measurements of SO_2 vertical profiles from the Vega-1 and Vega-2 landrs (Bertaux et al., 1996). The SO_2 was measured by its absorption along a path of 1.7 m, as recorded in the spectrum of the UV light of a xenon flash. Above 40 km, the two mixing ratio profiles are quite different, linked to the vertical structure of the clouds; the average value is in agreement with other previous measurements in this altitude range. Below 40 km, the profiles are very similar, exhibiting a steady decrease to lower altitudes, suggesting low values at ground level that would be compatible with chemical reactions with minerals.

Though night stellar occultations are preferred, it is important that some daytime occultations are performed, especially using bright stars on the bright limb. Mars Express showed that the pointing is so good that the star image can be placed with the 50 μm slit. The day-night amplitude variation of the exospheric temperature (at the top of thermosphere) is enormous on Venus (from 330K down to 100K at night) and is a crucial test for the validity of sophisticated thermospheric global circulation models, such as that developed by Bougher et al. (1990). SPICAV UV offers a fair cover of density/temperature profiles (local time, latitude and solar activity: there are no seasons on Venus, and geography is assumed to be irrelevant for the upper atmosphere) with which the Thermospheric General Circulation Model could be validated (or invalidated, and modified accordingly). Then, such a model could be used as a predictive tool for managing aerocapture/aerobraking operations in future.

Finally, the unique ability of SPICAV UV to detect condensation clouds during the night should be mentioned. On the nightside of Mars, in more than 60% of occultations, a distinct detached layer is found (Montmessin et al., 2006a): dust or water-ice cloud? In addition, SPICAM has seen in a few occurrences a high altitude layer: a CO_2 condensation cloud, according to the temperature retrieved simultaneously from the CO_2 vertical profile (Montmessin et al., 2006b).

2.6.3 SO_2 vertical profiling

SO_2 is the most important minor constituent of the atmosphere of Venus. It combines with H_2O to form the permanent thick cloud deck of H_2SO_4 droplets. The problem of its origin is pending. Thermochemical reactions with the surface minerals (Fegley et al., 1997) indicate that the mixing ratio in the atmosphere should be of the order of 5 ppmv. The fact that several descent probes found a mixing ratio of 180 ppmv at around 40–50 km has been used to suggest that SO_2 is of volcanic origin, and may be fairly recent. In such a case, one could dream of an atmosphere of Venus without clouds, and much cooler than now. Supporting this view was the measured decrease of SO_2 above the clouds over several years, as reported by Esposito (1984) from Pioneer Venus UV spectra, interpreted as a sign of current decline in SO_2 after an eruption some years (or tens of years) ago. However, two things have to be considered in the discussion. First, the 'ISAV' instruments on the Vega-1 and Vega-2 descent probes measured the actual vertical profile of SO_2 in the clouds, below the clouds and almost down to the surface. The SO_2 mixing ratio was found to be 50–200 ppmv at cloud level, and decreasing below, down to ~10 ppmv at 5 km altitude (Bertaux et al., 1996;

Fig. 20). Therefore, it indicates that indeed SO_2 could be in equilibrium with the surface. Second, SO_2 is destroyed very rapidly above the cloud by solar UV, and its density decreases very rapidly. Therefore, the SO_2 downward trend reported by Esposito (1984) could be a subtle change in the vertical structure of the clouds. By measuring SO_2 vertical profiles just above the clouds, and monitoring some possible changes, we may be able to understand the origin of the variations observed by Esposito.

2.6.4 The case for molecular oxygen

Molecular oxygen is the result of CO_2 photo-dissociation. O_2 provides an additional absorption in the Schumann-Runge bands (170–210 nm) that could be measurable. O_2 was discovered by its emission at 1.27 μm by Connes (1979) with Fourier transform high-resolution spectra taken at Palomar. However, this emission occurs, day and night, when O atoms produced by extreme-UV photo-dissociation of CO_2 recombine to form the O_2 molecule, much like the known NO emission on Venus and discovered recently by SPICAM on the night side of Mars. This is a quite different process of emission from the Mars atmosphere: photo-dissociation of ozone. This emission at 1.27 μm does not trace the density distribution of O_2 as would the UV absorption in the Schumann-Runge bands seen in occultation. The observation of the absorption band at 760 nm in the near-IR by SPICAV IR, either to the nadir or in solar occultation, could be a possibility.

2.6.5 Profiling and characterising atmospheric aerosols

Occultation spectroscopy is probably the most sensitive remote technique for sounding the vertical structure of clouds and aerosols. Above the thick cloud there is some light haze, the nature of which is not clear. Stellar and solar occultations will be used to characterise their quantity, size distribution and possibly their nature. In solar occultation, the information about the spectral continuum at distant wavelengths is a byproduct of gaseous absorption retrievals. As soon as the slant atmospheric opacities at different wavelengths are obtained from occultation data, the aerosol extinction will be retrieved by Abel inversion. Then, using Mie theory (possibly adapted for non-spherical particles), a number of unknown parameters characterising the aerosol component can be extracted, such as the size distribution and the real and imaginary parts of the refractive index. Also, the vertical variation of key parameters, such as the effective radius and the particle number density, will be retrieved. Observations of solar light scattered at the limb will also be useful in this respect, as it is for Mars with SPICAM. In both cases, SPICAM has determined (Montmessin at al., 2006; Rannou et al., 2006) a large variability of the Angström coefficient α, which describes the continuous absorption of dust/aerosols as a power law of the wavelength, $\lambda^{-\alpha}$. This coefficient is related to the size of the particles, which is submicronic (down to 0.1 μm radius) when α is large (~3 to 4).

2.7 Solar occultation measurements

In addition to stellar occultations performed by the UV channel, all three SPICAV spectrometers will benefit from solar occultations by Venus. There is a special solar-light aperture at 90º to the +Z axis (the common axis of the optical instruments), so it can be pointed towards the Sun by orienting the spacecraft without disturbing the optical instruments. On Mars Express, this has proved to be no more difficult an attitude control task than keeping nadir orientation, or pointing at stars. The angular diameter of the Sun as seen from Venus is 0.7º, but since the brightness of the solar disc is not uniform in the UV, attitude control stability is desirable (and well-achieved on Mars express). There is no precession of the orbit plane, and during one Venusian year, there are two periods of solar occultations. The latitude of the occultation varies between +80º and –45º, as

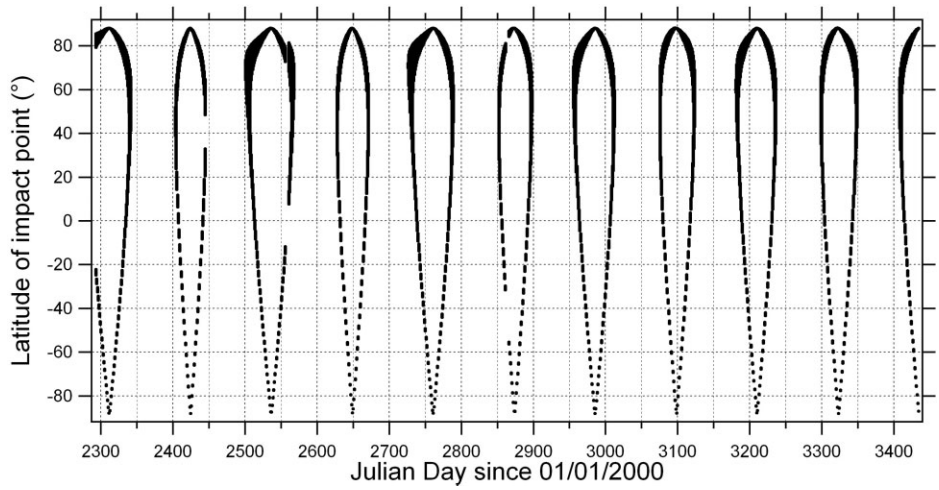

Fig. 21. Variation of the latitude of the Venus point where the solar occultation occurs over a 3-year period. There are two 'seasons' of solar occultation per Venusian year.

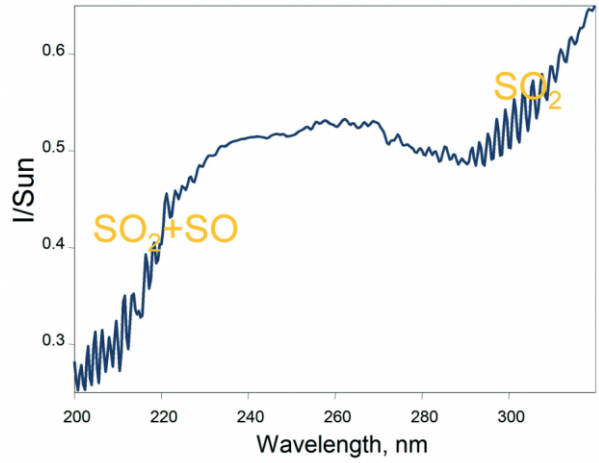

Fig. 22. Synthetic UV albedo spectrum of Venus at 0.4 nm resolution (computed by L. Zasova). The most prominent absorptions are those of SO_2; the short wavelength absorption is also due to SO.

seen in Fig. 21, offering a fair latitude coverage. SOIR will work essentially within these periods, and should have the highest priority.

Solar occultation spectroscopic sounding of planetary atmosphere has several advantages over other methods of remote atmospheric sensing. Solar radiation is an incomparably powerful source traversing the atmosphere, providing the largest possible atmospheric path. The air-mass factor reaches 40–45 for Venus. As for stellar occultations, the measured spectra are compared with unattenuated signal from the atmosphere, which is measured in the same sequence prior to occultation. No absolute calibration is necessary. A drawback of the solar occultation technique is that the atmosphere can only be observed when and where a sunset/sunrise occurs.

The vertical resolution of the UV channel in solar occultations is determined by the slit width in one direction and by the pixel height in the other, and by the distance to the limb, which varies with time. Some periods are therefore more favourable to get good vertical resolution. Assuming that the spectra are integrated over two lines of the CCD, the FOV is 1.5 x 1.5 arcmin, which leads to a spatial resolution of 1.5–3 km. If the spectrum from a single CCD line is considered, the metric resolution could be doubled for one coordinate. The FOV of the IR channel will be quite large owing to simplified and miniaturised fibre optics that deliver solar light to the IR: about 4 arcmin, limiting the vertical resolution at the limb to 4 km under the best conditions.

The UV channel in the solar mode will pursue all its scientific targets in the

stellar occultation mode at the terminator with a better signal-to-noise ratio, except below 190 nm, where the solar spectrum is weak. Owing to the Sun's high brightness, deeper sounding is possible in the upper cloud deck. The near-IR channel, thanks to the solar occultation sounding, can measure vertical profiles of water vapour, complementing the more accurate measurements of SOIR.

As suggested by Hassler (private communication), slowly slewing the spacecraft when looking at the Sun with SPICAV UV would allow a spectro-heliogram to be produced, revealing active areas on the solar surface. Thus the face of the Sun invisible from Earth for long periods could be monitored, providing advance warning of active areas for Space Weather forecasts.

2.8 UV nadir measurements

2.8.1 Dayside measurements

On the dayside, measurements are made of solar light scattered by the gaseous atmosphere (Rayleigh scattering) and by the particle in the clouds and hazes, modified by absorption of CO_2 (at $\lambda < 200$ nm), and by some other gaseous and particle absorption. When divided by the incoming solar spectrum, the nadir spectrum gives the albedo. Fig. 23 is the calculated albedo of Venus in the UV, taking into account absorption by SO_2 and SO. As demonstrated with Mars Express, the UV sensitivity of SPICAV, blind in the UV > 320 nm and visible, will allow the absolute value of the spectral albedo at 110–310 nm to be measured more accurately. SPICAV UV is regularly calibrated by observing the stars before occultations. The absolute solar spectrum outside the atmosphere is well known. Therefore, the albedo spectrum of Venus can be obtained with a good absolute accuracy and at a spectral resolution of 1.5 nm. Then, comparing this spectral albedo to forward models using radiative transfer simulation codes (as for Mars Express, Perrier et al., 2006), a quantitative estimate of SO_2, perhaps SO and other absorbers could be retrieved. The problem is not trivial, though, for a number of reasons. One is that the vertical distribution of particles may be poorly constrained (the occultation measurements will be useful, but not able to probe down to a vertical optical depth of 1, as would be desirable). The other is that the cloud deck is horizontally non-uniform. Indeed, the UV albedo of Venus is horizontally structured, which led to the discovery of the 4-day rotation of the cloud-top atmosphere (Boyer & Camichel, 1965). In spite of many efforts, the exact nature of the UV absorber is still unknown (Bertaux et al., 1996). Is it the same substance that also absorbs in the blue part of the spectrum? Is it in the gaseous phase, or in the cloud droplets? An answer to this irritating question could come from the detailed comparison of blue-filter images from VMC and SPICAV UV along-track measurements. While the retrieval from radiative transfer codes might be uncertain, horizontal variations will tell us a lot about the structure of the clouds. Finally, the nightside IR emission has also been found to be highly structured horizontally: the IR radiation from the ground and lower atmosphere is strongly variable, suggesting a variable thickness of the cloud. A hole detected in the nightside can be observed 2 days later on the dayside; it will be interesting to see if there is any correlation with the UV albedo.

2.8.2 Nightside nadir measurements in the UV

In the wavelength range of SPICAV UV, the main emissions detected are: H Lyman-alpha, the γ and δ bands of nitric oxide produced by radiative recombination, and auroral emissions. Here, the case of H Lyman-alpha, which is directly connected to the thermosphere temperature, is discussed briefly. The thermosphere of Venus is somewhat extraordinary, because it varies from day to night over a wide range, from ~300K on the dayside to ~100K on the nightside. Therefore, the whole upper atmosphere is 'retracted' vertically on the night side. As a result, the coronal H is also retracted, and there is little transport of solar Lyman-alpha from the dayside (where they are scattered by H atoms) to the

nightside. Coupled with the very low temperature, provoking a narrower H linewidth, it makes the nightside of Venus very dark in Lyman-alpha, as observed by Venera-9 and -10 (Bertaux et al., 1979). It is possibly the darkest place in the Solar System in Lyman-alpha: much darker than the interplanetary medium at any rate. With Venus Express, there are many opportunities to study in detail this weak emission on the nightside. Possibly the source of emission is mainly the backscattering of interplanetary photons. If so, it should vary as a function of the Venus ecliptic longitude, when the Doppler shift between Venus (including its orbital velocity) and the interplanetary flow of interstellar H are zero. In this respect, it would be useful to measure from time to time this Lyman-alpha interplanetary emission from apocentre, in various directions.

Finally, comets are interesting targets of opportunity, bearing in mind that Venus might be in a much better position in the Solar System than Earth for observations. Comet 45/P Honda Mrkos Pajdusakova will indeed come within 0.085 AU of Venus, and an observation campaign with Venus Express instruments will be organised.

3. Near-IR Spectrometer

3.1 The nightside IR emission of Venus

The remarkable discovery of bright near-IR markings on the nightside of Venus (Allen & Crawford, 1984) was made more then 20 years ago. Since then, these features have not been observed by any spacecraft, except for brief observations during the Galileo and Cassini flybys. At night it is possible to observe radiation in several spectral ranges (near 1, 1.23, 1.74 and 2.3 μm; Fig. 23) originating from different altitude levels below opaque clouds, down nearly to the surface (at 1.0 μm). Spectral analysis of this radiation provides the unique possibility for remotely accessing the deep levels of the atmosphere. VIRTIS will perform imaging and mapping in these windows, and SPICAV IR will analyse the nightside spectra at a high spectral resolution (comparable to the high spectral resolution channel of VIRTIS, with somewhat more flexibility and less data volume collection).

The SPICAV IR channel is derived from the very successful SPICAM IR of Mars Express, a miniature IR spectrometer based on AOTF technology. The scientific goals of SPICAV IR at Venus are:

— the study of H_2O and aerosol vertical distribution (solar occultations);
— the determination of the H_2O abundance above the clouds (nadir, dayside);
— the monitoring of the 0.76 μm and 1.27 μm O_2 emissions (limb);
— sounding the surface in the 0.8–1.0 μm windows (nadir, nightside);
— measurements of H_2O content near the surface (nadir, nightside);

3.2 Technical description of the AOTF IR channel

SPICAV IR is a single-pixel spectrometer for the spectral range 0.7–1.7 μm with a spectral resolution of 3.5–8 cm^{-1}, based on AOTF technology. It will sequentially measure the spectrum of reflected solar radiation from Venus on the dayside and the emitted radiation in spectral windows on the nightside with a coarse spatial resolution of 10–15 km. Mars Express demonstrated the AOTF approach on deep space missions. For Venus, the spectral range is extended to 0.7 μm with enhanced sensitivity in the entire range, especially at 0.7–1.1 μm to measure the radiance from the atmosphere below the clouds and the surface of Venus on the nightside. These measurements will complement the low-resolution spectral mapping by VIRTIS in the same spectral range. An important goal of the IR modification is to measure the H_2O content below the clouds on the nightside. The dynamic range between the dayside and night side measurements is very large, so increased sensitivity and much longer exposures are required. As with SPICAM, the AOTF configuration conserves both polarisations, thereby

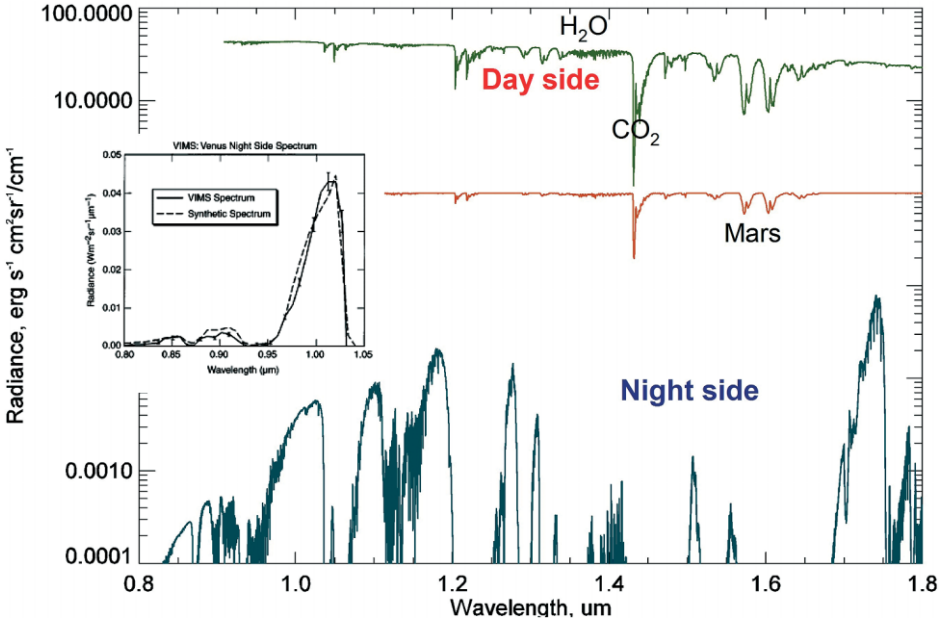

Fig. 23. Synthetic spectrum of the Venus nightside emission (computed by N. Ignatiev) at the spectral resolution of SPICAV IR compared to the spectrum of reflected solar radiation on Venus and Mars. Note the dynamical range of 4.5 orders of magnitude between the dayside and nightside observations. The Cassini/VIMS spectrum (Baines et al, 2000) is shown for comparison.

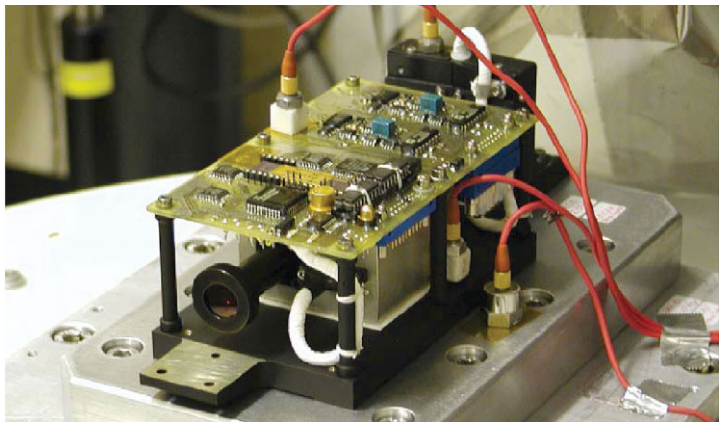

Fig. 24. The SPICAV IR channel under vibration testing. The telescope is at the front; the grey metallic box is the AOTF unit. The detector unit is to the rear.

allowing spectro-polarimetry measurements. A fibre-coupled solar entry allows profiling of the Martian atmosphere using solar occultations. The AOTF devices, based on Bragg diffraction of an entrance beam on the ultrasonic acoustic wave excited within a crystal, are new. They offer the potential of a resolving power of better than 1000, ample to measure H_2O towards the nadir by scanning the absorption line at 1.38 μm in the reflected solar spectrum. There are no moving parts.

SPICAV is shown in Fig. 24; its principal characteristics are given in Table 3. As in SPICAM, the SPICAV IR spectrometer is mounted alongside the UV spectrometer. The AOTF employs a tellurium dioxide crystal in the non-collinear configuration, producing two polarisations of the diffracted light. The diffracted beams are deflected at a small angle with respect to undiffracted 'white' output beams. When the acoustic wave is turned on, two diffracted beams appear. These two weak beams need to be separated from each another and from the strong undiffracted beams, which contain most of the spectrum. The active zone of the AOTF crystal is 25 mm across. Two detectors with proximity lenses capture the ordinary and extraordinary beams. The undiffracted central beams are captured by a light trap.

The Venus requirements for spectral range, sensitivity and dynamic range led

Table 3. Characteristics of the SPICAV near-IR channel.

	Short Wavelength	*Long Wavelength*
Spectral range	0.65–1.05 μm	1.05–1.7 μm
Spectral resolution	0.42 nm at 630 nm 1.44 nm at 1050 nm	0.55 nm at 1.05 μm 1.5 nm at 1.7 μm
FOV	2° circular	
Telescope	Lens type, ŕ12 mm; focal length 40 mm	
AOTF	TeO_2, two actuators, aperture 6x4 mm, 2°	
RF frequency range	140–250 MHz	80–140 MHz
Detector	Two bicolour diodes (Hamamatsu K3413-05) 1 stage TE cooled to –15°C	
	silicon 2x2mm	InGaAs 0.5 mm dia
Transmission of optics	~20%	
NER (erg $s^{-1}cm^{-2}sr^{-1}\mu m^{-1}$)	0.05	0.15
Gain control	4 pre-chosen gain values	
Integration times	0.7, 1.4, 2.8, 5.6, 11.2, 22.4, 44.8, 89.6, 179.6 ms	
Number of spectral points	2 spectra with different polarisations, 664 points each	
Dynamic range	2^{24}, packed into 2^{12}	
Power consumption	1.5 W average at 28V	
Data rate:	6.2 kbyte per spectrum	
Dimensions	220x85x65 mm (excluding DC/DC and DPU)	
Mass of the IR unit	700 g (excluding DC/DC and DPU)	

to deep modifications of the spectrometer (Korablev et al., 2002b,c). To extend the spectral range from 1–1.65 μm to 0.7–1.65 μm, a second, short-wavelength actuator was added. The single TeO_2 AOTF crystal, similar to that in SPICAM, now has two piezoelectric actuators, one for 0.7–1.1 μm and the other for 1–1.7 μm. The actuators are fed from two separate radio-frequency (RF) amplifiers, using a common programmable RF synthesiser with two outputs (f and $2f$). For testing, the short-wavelength channel reaches the wavelength of the red HeNe laser at 633 nm, but the AOTF efficiency at this extreme wavelength is low. The sensitivity of InGaAs photodetectors below 1.1 μm is poor, so another detector was necessary for the short-wavelength channel. In place of the Hamamatsu InGaAs G5832-11 1 mm-diameter photodiodes used on Mars Express, Hamamatsu K3413-05 two-colour sandwich detectors are employed. The electrically-cooled detector consists of a silicon 2x2 mm photodiode on which is superimposed a InGaAs 0.5 mm-diameter photodiode.

Several factors allowed improvements in the sensitivity and the dynamic range. First, the silicon photodiode and the smaller InGaAs photodiode are less noisy than the original 1 mm InGaAs detector. Further treatment of the signal is completely new. Each photodiode feeds current to a low-noise integrating preamplifier IVC102 (TI & Burr-Brown), followed by variable amplification stages and then an integrating amplifier. Spectral points are measured sequentially. The measurement sequence of one spectral point is shown in Fig. 25.

First, the AOTF frequency can be updated for each measurement. At this point, the RF power is not applied to the AOTF transducer, so the useful optical signal at the AOTF output is zero (AOTF is OFF). Then preamplifiers integrate

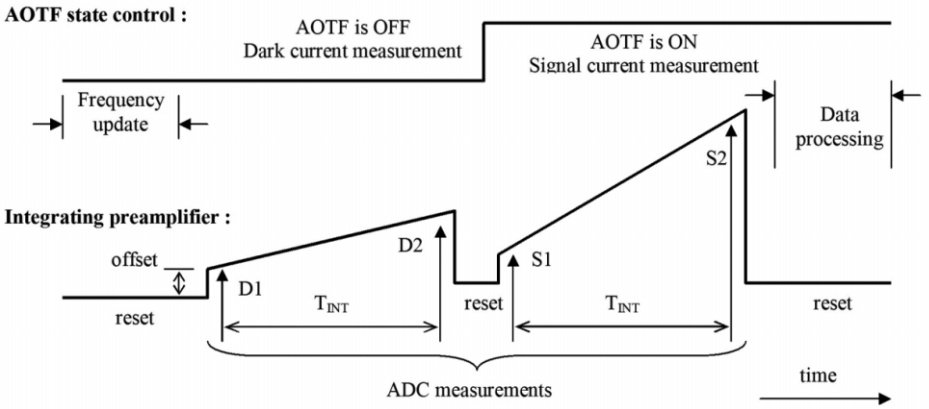

Fig. 25. The basic sequence of SPICAV IR measurements.

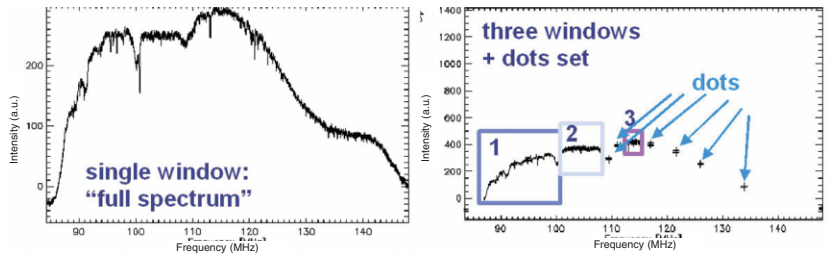

Fig. 26. The SPICAM IR operation modes. Left: a full spectrum, when the AOTF driving frequency spanning the entire range and the AOTF is sequentially tuned to all wavelengths from 1 μm to 1.7 μm. With a fine sampling, such a sequence requires several seconds (12–24 s, depending on integration time, etc.). Right: the optimised sequence, in which only the interesting portions ('windows') of the spectrum are scanned at maximal sampling, the less important are scanned with reduced sampling, and the rest of the spectrum is characterised by only few continuum points ('dots').

dark current and two measurements (D1 and D2, separated by time T_{INT}), made at the beginning and end of this integration interval. In order to eliminate signal offset produced in the electronic circuit, the difference D = D2–D1 is calculated; D is proportional to the sum of dark current and straylight current. Then, the RF power is turned on (AOTF is ON) and two measurements of signals S1 and S2 are performed in the same manner. The difference S = S2–S1 is proportional to the sum of the dark current, straylight current and diffracted light current. Finally, the difference R = S–D is controlled; this is proportional to the useful diffracted light current only. Integration time T_{INT} is determined by software and varies from 0.7 ms to 179.6 ms (c.f. 1.3–12.8 ms for SPICAM). The procedure is applied to both measurement channels simultaneously and every frequency point.

Optically, the entry telescope was simplified by enlarging the FOV angle from 1° to 2°. The long integration time required special care with straylight, and the smaller near-IR detector required greater care in focusing the output beams. The near-IR channel, for solar occultations, uses a solar aperture near the solar entry of the UV spectrometer. An optical fibre delivers the solar light to the objective. The fibre's optics provide an angular FOV of about 4 arcmin. A collimator lens at the fiber output and a 45° flat mirror mounted at the baffle of the near-IR objective complete the design of the solar entry for the IR.

The frequency of the AOTF's ultrasonic excitation is controlled by software, so the choice of the AOTF wavelength is free within the spectral range. Then only the most important and interesting parts of the spectrum can be measured with the desired sampling. During the first orbits at Venus, it was planned that the AOTF's full range would be used, to acquire full spectra at maximum sampling, at the expense of longer sampling intervals. Then, after an initial analysis, the spectra were to be restricted to the most interesting parts, with a great variety of spectral samplings, through three windows and a number of dot spectral points to cover the full range (Fig. 26).

The ordinary and extraordinary beams at the output of an AOTF crystal can be analysed simultaneously with two identical detectors, and the polarisation of the incident light can be measured with high accuracy (Glenar et al., 1994).

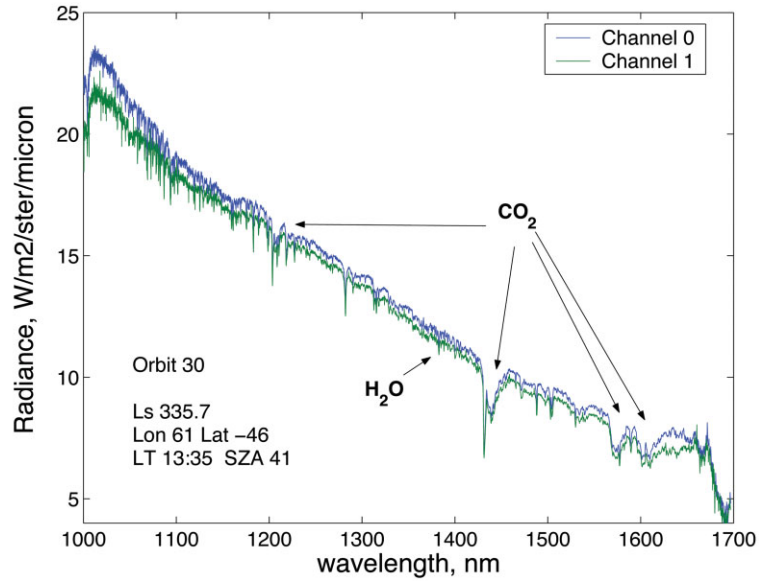

Fig. 27. An example of a calibrated SPICAM IR spectrum for Mars Express orbit 30. Individual spectra for two different polarisations are shown.

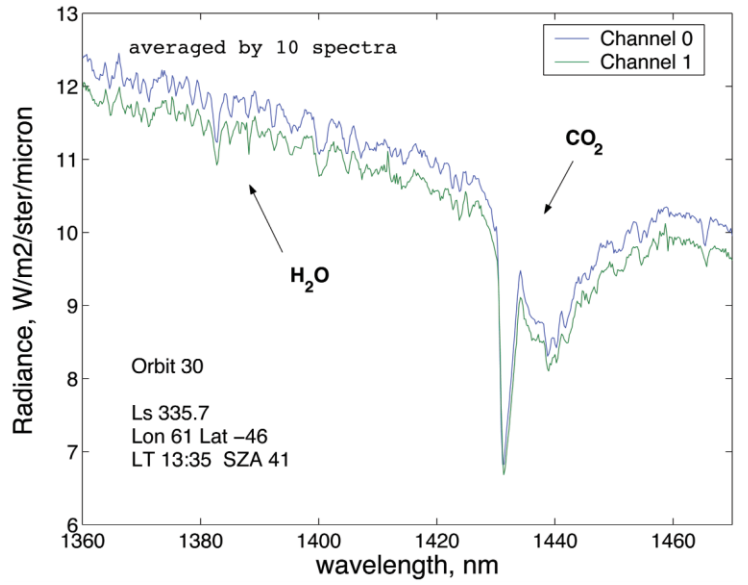

Fig. 28. A portion of the spectrum from Fig. 27, showing the vicinity of the H_2O absorption band at 1.38 μm, and the adjacent CO_2 band at 1.43 μm. For a clear representation of the complicated H_2O band, 10 subsequent spectra (1 s each) of orbit 30 are averaged.

Polarimetry measurements enable a characterisation of the properties of the atmospheric aerosol component (Santer et al., 1985). The spectral measurements by the SPICAV near-IR channel can be used for cross-validation of VIRTIS and PFS data.

3.3 Operations and capabilities

Results obtained from the Mars Express AOTF spectrometer illustrate the capabilities on Venus Express. Owing to the nature of the AOTF sequential measurements from a spacecraft orbiting a planet, each measured spectral point generally corresponds to a different spot at the surface. The FOV of 1° corresponds to ~5 km from the Mars Express pericentre, so it is therefore desirable to restrain the overall duration of the measurement of the whole spectrum to 5–10 s. However, the full scan of the spectral range at fine spectral sampling (3–4 points per element of the AOTF spectral resolution) requires almost 4000 points; with a reasonable integration time of 6 ms, this leads to 24 s measurements. The AOTF can be randomly tuned to any wavelength within the

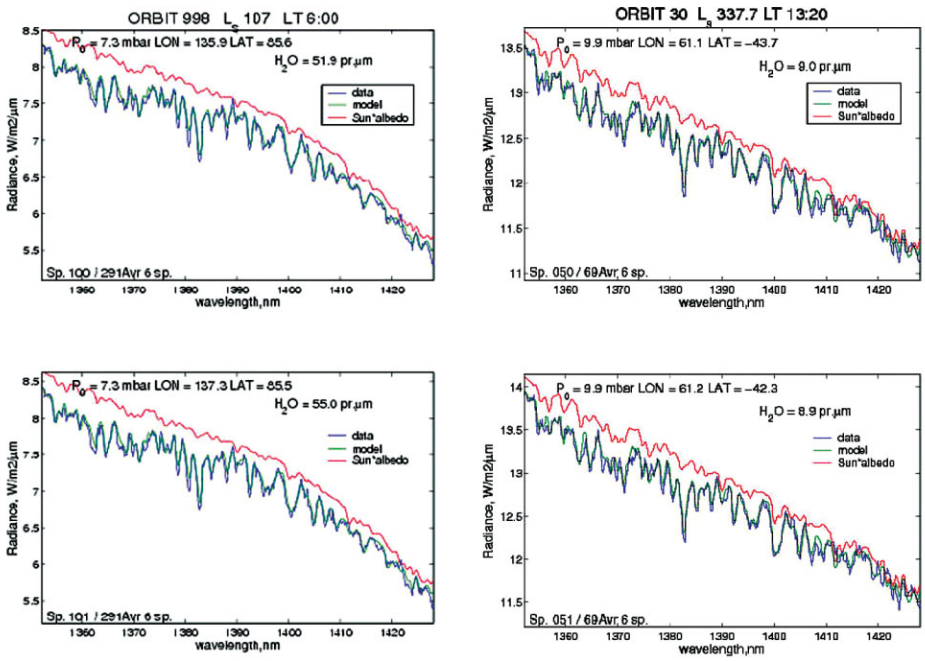

Fig. 29. Examples of fits to the SPICAM IR data in the H_2O absorption band at 1.38 µm. Blue curve: calibrated data taken at nadir orbit 998; green curve: synthetic fit; red curve: the solar spectrum modified by surface albedo and continuum atmospheric extinction.

spectral range, allowing the measurement time to be optimised without compromising the science return. The IR spectrometer can be programmed to scan up to three windows, and to determine for each the bounds and the spectral sampling. Furthermore, several sets of predefined 'dots' are available to characterise the spectral continuum (albedo of the surface, reflectance at limb, extinction, etc.). During the commissioning phase of Mars Express, a number of complete spectra were recorded first, and then the parameters of the optimised window-dot sets for different observation modes were defined. Also, parameters such as gain and AOTF power were optimised.

3.3.1 Water vapour

A typical calibrated spectrum measured by SPICAM IR at nadir for early orbit 30 is presented in Fig. 27. The main features of the spectrum are the spectral slope towards the longer wavelengths owing to the solar spectrum, a large number of Fraunhofer lines, and some atmospheric absorption features, the most prominent being the CO_2 absorption bands at 1.43, 1.58 and 1.6 mm, and the H_2O absorption band around 1.38 µm (Fig. 28).

The latter band (Fig. 28) was used for the routine retrieval of the total column water vapour abundance in the atmosphere of Mars; each individual spectrum in the sequence is generally used. An important issue is an accurate solar spectrum, because numerous solar lines frequently mix with the signatures of the Martian atmospheric gases. There are few sources for a high-resolution solar spectrum in the range of interest; for the moment, the spectrum by Kurucz et al. (1995) is used, although its resolution (sampled at 1 cm^{-1}) is at the limit of what is required.

Examples of synthetic fits to the SPICAM IR measurements are presented in Fig. 29. To measure the atmospheric water vapour, a synthetic spectrum is fitted to the data; the retrieved quantities being water vapour total column amount in precipitable microns, and the modification of the spectrum owing to non-gaseous extinction and reflectivity of the surface of Mars. Folded with the solar spectrum, this function is denoted as the Sun's albedo in Fig. 29.

3.3.2 Oxygen $O_2(^1\Delta_g)$ emission

On Mars, the emission of the dayglow 1.27 µm $O_2(^1\Delta_g)$ is produced when O_3 is

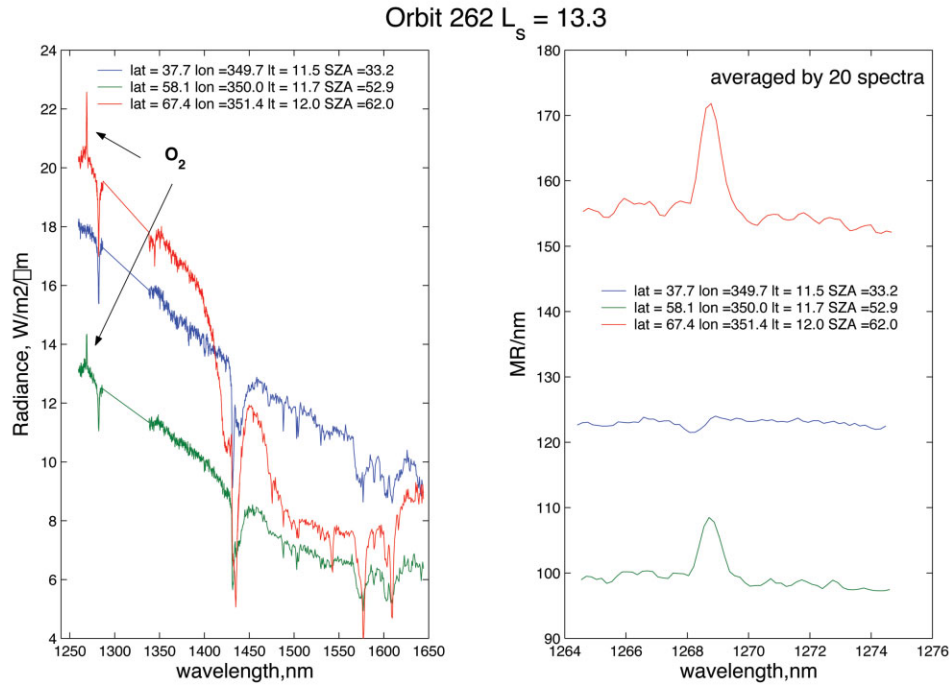

Fig. 30. Three spectra measured by SPICAM IR along orbit 262 for latitudes 38º (blue), 58º (green) and 67º (red). At right is the enlarged region of 1.27 μm O_2 ($^1\Delta_g$) emission band.

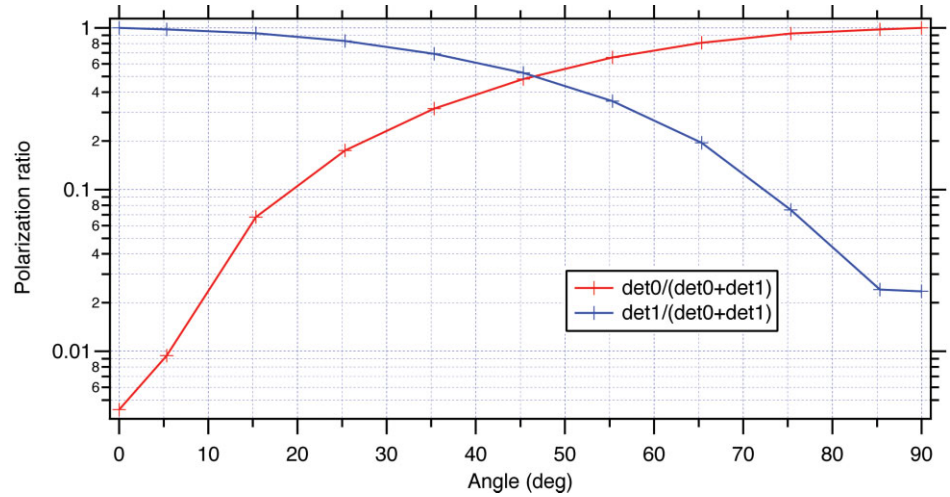

Fig. 31. Laboratory calibration: the output of both SPICAV IR channels is plotted as a function of the angle of a rotatable polariser. The outputs are divided by the total flux, which is the sum of both channels.

photo-dissociated by solar UV into O+O_2. The O_2 molecule is produced in an excited state, which de-excites spontaneously while emitting a photon at 1.27 μm

The band intensity observed by different authors from the ground varies from 1.5 MR to 26 MR on Mars; indeed, SPICAM IR routinely observes the $O_2(^1\Delta_g)$ band at nadir and on the limb of Mars, mostly in the polar regions. Three spectra recorded along one orbit at different latitudes are different (Fig. 30): the albedo is different, the shape of the spectrum, and the shape of CO_2 absorption of spectrum 3 lines differ from 1 and 2 (see below), and finally, an emission feature near 1.27 μm is apparent in spectra 2 and 3. This region zoomed at the right panel of Fig. 30 reveals a clear signature of the $O_2(^1\Delta_g)$ band of the Martian atmosphere. Venus has the same emission but it occurs day and night, when O atoms produced by extreme-UV photo-dissociation of CO_2 recombine to form the O_2 molecule. This is a major way to study upper atmosphere circulation, together with the NO emission in the UV (N+O recombination).

3.3.3 Polarisation

Variations of polarisation with wavelength and phase angle are useful for determining characteristics of aerosols in the upper part of the clouds, and in the upper haze, if observed at the limb. However, because of the rather large 2° FOV, the spatial resolution at the limb is coarser than desirable. The polarisation power of the SPICAV IR spare Flight Model was measured; each channel is totally polarising, and they are orthogonal.

4.1 The scientific question of HDO and H_2O in the upper atmosphere of Venus

The present value of the D/H ratio says something (but not everything) about the history of water on the planet. Deuterium in the lower atmosphere is ~150 times more abundant on Venus than on Earth (Donahue et al., 1997; De Bergh et al., 1991). This enrichment of D/H is explained by preferential escape of H atoms from the upper atmosphere, with ion escape (H^+ and D^+) also important. The present water content and D/H ratio can be interpreted either as the signature of an equivalent 3 km-deep primordial ocean, lost at present (mainly by hydrodynamic escape), a steady state in which water is continuously supplied to the surface by comets or volcanism, or a non-steady regime combining the two sources. The present lifetime of the atmospheric water is highly uncertain but is likely less than 100 Myr, so the primordial ocean is probably not the sole source of the present water. It may, however, be possible to derive constraints on the primordial water abundance by measuring precisely the atmospheric escape of water (i.e. of H atoms), and the fractionation factor describing the efficiency of D escape relative to H escape (Gurwell, 1995). The escape rate of D and other atoms from the planetary exosphere depends, first, on their abundance in the upper atmosphere and, second, on the peculiarities of the interaction of the solar wind with the atmosphere. While escape of hydrogen is approximately known, the abundance of deuterium in the upper atmosphere and its escape rate are poorly constrained by optical observations (Bertaux & Clarke, 1989), though mass 2 ion measured by the ion mass spectrometer on Pioneer Venus is proposed to be D^+, instead of H_2^+, as originally claimed (see the discussion above in the SPICAV UV section). The measurements of atom abundance and their vertical profile would be extremely important for quantifying the escape processes. SPICAV UV might not be able to detect the D atom's Lyman-alpha spike at the limb. However, the quantity of D^+ ions, of D atoms at escape level, and the D and D^+ escape rates, are certainly proportional to HDO abundance at the homopause level (~100 km). Therefore, the measurement of HDO as high as possible will give quantitative indications on the present escape rate of D atoms.

4. SOIR Spectrometer

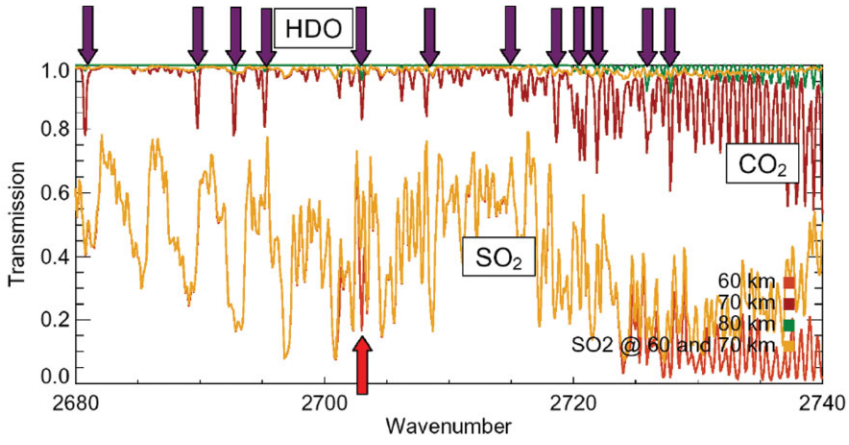

Fig. 32. Simulation of the atmospheric transmission of Venus for various tangent altitudes of the LOS. At 60 km, SO_2 absorption contaminates HDO, but in this model the quantity of SO_2 is somewhat exaggerated. One line of HDO can be detected (red arrow) at 60 km. HDO is very well measurable at 60–70 km, in the region where the 'cold trap' may exist. In this simulation, a mixing ratio of 5 ppm was assumed for H_2O, and HDO/H_2O = 120 times terrestrial.

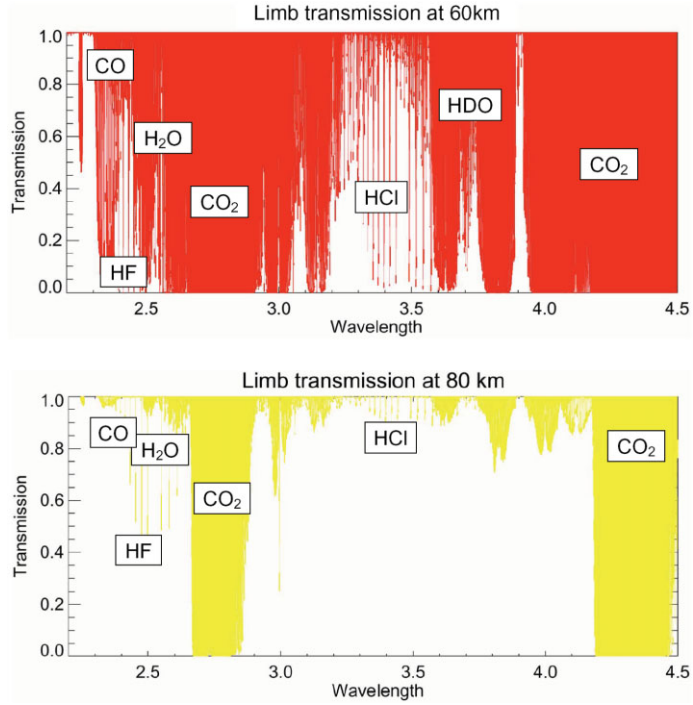

Fig. 33. Computed limb transmission of the atmosphere at grazing altitudes of 60 km and 80 km, in the wavelength domain of SOIR. Various gases are absorbing in different wavelength regions.

SOIR will measure HDO profile up to 80–90 km, thereby characterising the escape of deuterium. Fig. 32 is a simulation of the atmospheric transmission of Venus for various tangent altitudes of the LOS. At 60 km, SO_2 absorption contaminates HDO, but in this model an SO_2 mixing ratio of 150 ppm was assumed at this altitude, which is somewhat exaggerated because photolysis destroys SO_2 above the clouds. Still, one line of HDO can be detected (Fig. 32, red arrow). Higher up, HDO is very well measurable at 60–70 km, in the region where the 'cold trap' may exist.

On Venus the dense atmosphere with opaque clouds at 45–60 km prevents deep penetration by solar occultation sounding. High-resolution occultation studies are possible above the clouds, in the upper-cloud layer (< 90 km) and higher. It allows unique measurements related to the escape of water, and thus to the evolution of water on the planet. Another important scientific objective for SOIR is the measurement of the water vapour abundance profile up to 100 km. In the range 60–70 km, this measurement can be performed in the band around 2560–2570 cm^{-1} (3.9 μm), which is expected to be unobstructed by any other absorbing constituent. The availability of the stronger 3760–3860 cm^{-1} (2.56 μm) absorption band allows the extension of water vapour observations up to 100 km. At an altitude of 60 km, the H_2O spectrum in this band shows few spectral lines unaffected by the absorption lines of CO_2 and HF, but at higher altitudes some isolated and useful H_2O lines become available. Other scientific targets of SOIR on Venus are: precise H_2O profiling up to ~105 km; measurements of atmospheric density up to very high altitudes, though complicated due to non-local thermodynamic effects; measurements of CO_2 and H_2O isotopes (besides HDO); measurements of known minor constituents (CO, HF, HCl, SO_2, H_2S, OCS); sensitive search for new minor species (C_2H_2, CH_4, NO, N_2O, H_2CO, HCN and many others). Further simulations of the atmospheric transmission in the SOIR total bandwidth are shown in Fig. 33.

4.2 Technical description of SOIR spectrometer channel

A full description of this novel instrument may be found in Nevejans et al. (2006).

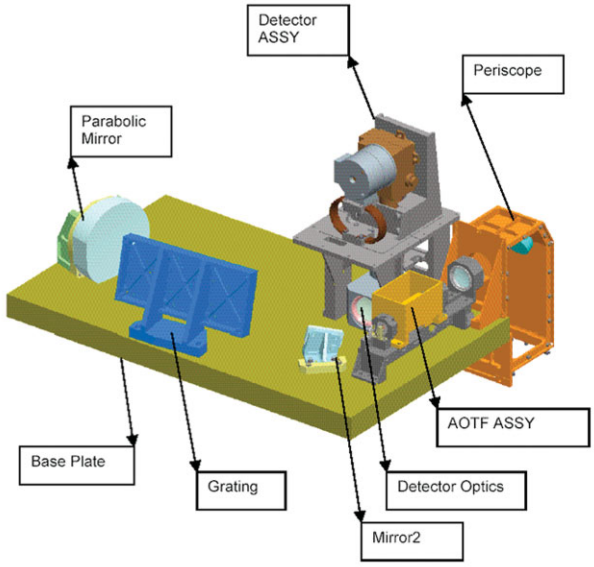

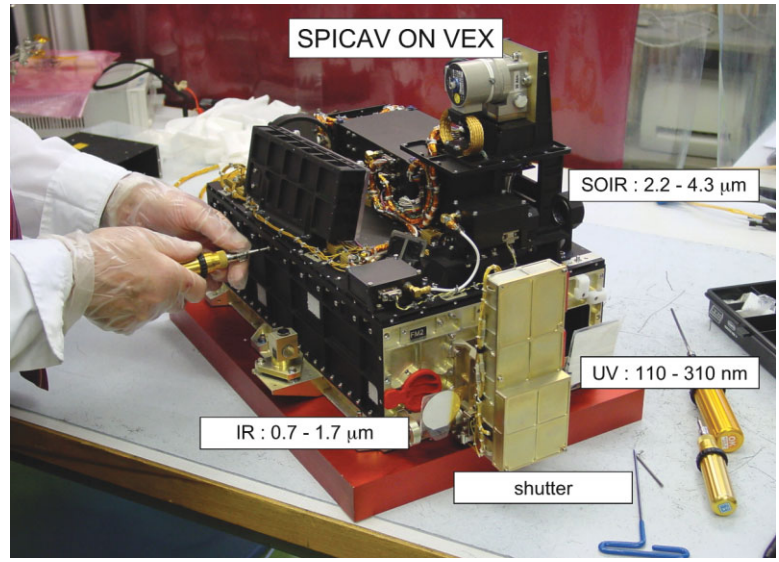

Fig. 34 (above left). The layout of the SOIR floor.

Fig. 35 (above right). The SOIR Flight Model (cover removed) mounted on top of the first floor containing the SPICAV UV and IR channels. At the front is the double shutter of the apertures.

Fig. 36 (below left). SOIR's simplified optical scheme.

Fig. 37 (right). A more detailed view of SOIR's optical scheme, as designed by OIP.

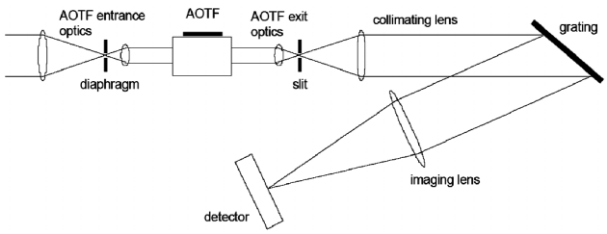

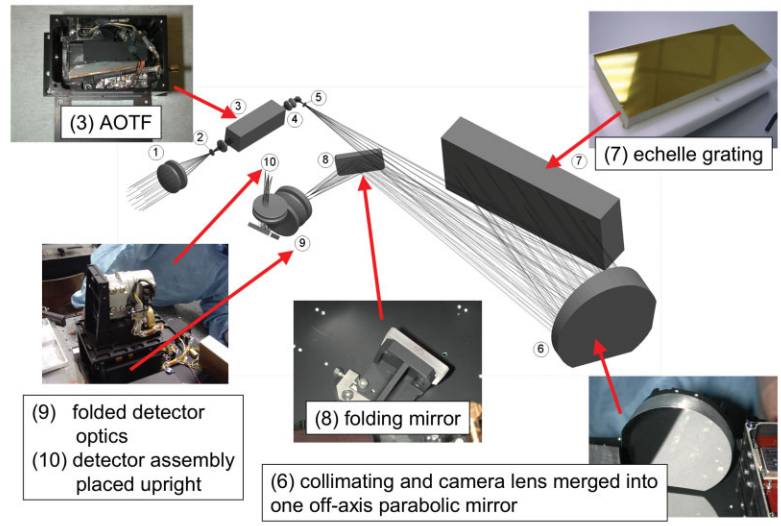

Fig. 34 shows the layout of the SOIR floor; Fig. 35 shows the SOIR Flight Model.

The SOIR optical concept uses an echelle grating to give higher resolution and dispersion than ordinary gratings, to yield high reciprocal dispersion and high throughput in a compact design. Since the echelle has overlapping orders, order-sorting is performed by an AOTF, which has the advantage of no moving mechanical mechanisms (unlike the classical solution of a filter wheel). An AOTF introduces the possibility of rapid random access to any grating order by command. As with SPICAV IR, deactivating the AOTF stops solar input to the spectrometer, thus measuring a thermal background spectrum that can be subtracted from the observed spectrum (no need of a mechanical chopper). Fig. 36 shows the simplified set-up of the compact high-resolution spectrometer using an AOTF-echelle combination; Fig. 37 shows a more realistic scheme. The spectrometer consists of three main parts: the front-end collects the solar light, defines the FOV and selects the observed wavelength domain; the spectrometer itself realises the desired spectral sampling interval and the spectral resolution; the detector system records the spectra.

The front-end starts at the AOTF entrance optics that reduce the diameter of

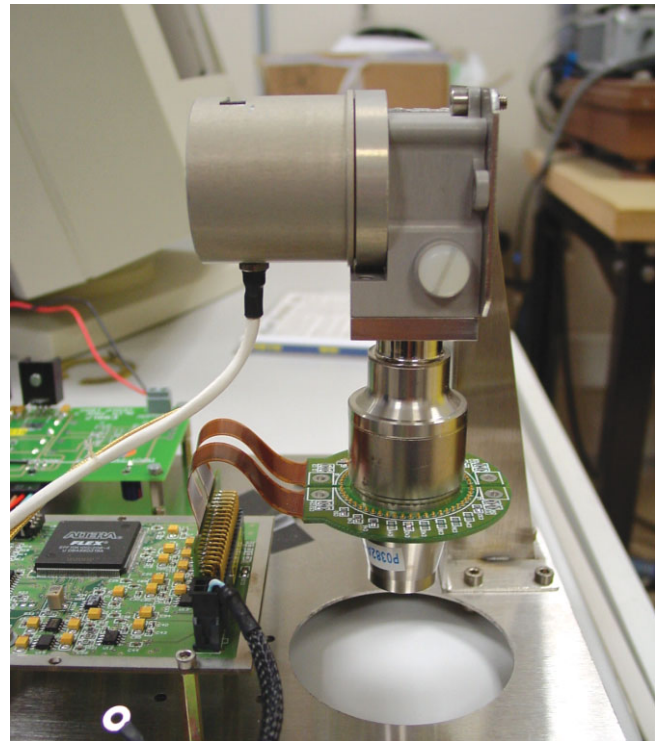

Fig. 38. Sofradir detector type ID MM067, integrated in a vacuum dewar and with a 0.4 W K508 integrated Stirling-cycle rotary microcooler from Ricor (Israel) / L'Air Liquide (France). This type of device was qualified for CIMEX and Clementine; the microcooler was qualified for VIRTIS/Rosetta. Mass is < 600 g.

the incoming light beam so that it is compatible with the AOTF acceptance aperture. For the solar light to enter along the optical axis, a 2-mirror periscope is mounted externally at the entrance of the spectrometer. In the entrance optics intermediate image plane, a diaphragm limits the FOV to slightly larger than the desired FOV, in order to block unwanted light and to avoid light scattering and ghost images. Then the beam enters the AOTF as the order-sorting filter of the system. When AOTF is ON, it directs a small spectral fraction of the incidence beam along its optical axis, aligned to the 'free spectral range' (the range of wavelengths in which there is no interference or superposition of light from adjacent orders). The AOTF exit optics image the beam on the spectrometer entrance slit. The slit is the entrance aperture for the spectrometer part of the instrument. A collimating lens captures the light passing through the slit and forms a parallel beam to the echelle grating, used in a near-Littrow configuration. Finally, the light diffracted by the grating is imaged via a camera lens on the detector. With 4 grooves per mm, the arctan(2) incidence grating spectrometer operates on diffraction orders from 101 (corresponding to the wavelengths of ~4.4 μm) to 194 (~2.3 μm).

The principal components of the instrument are:

— custom AOTF from AFAR, Russia (Table 4);
— custom echelle grating from Bach Research, Boulder, USA (Table 5);
— customised 2-D HgCdTe ID MM0067 detector from SOFRADIR, France (Fig. 38).

SOIR is controlled by a dedicated space-qualified FPGA-based electronics unit, designed by BIRA-IASB.

The customised version of the ID MM0067 contains an IR optoelectronic device sensitive to 1.7–4.3 μm, although a window filters it to 2.2–4.3 μm. The device includes a high-sensitivity focal plane array of a 2-D detector array made of photovoltaic HgCdTe (mercury-cadmium-telluride; MCT) pixels organised as

Table 4. Characteristics of the SOIR AOTF.

Material	TeO_2
Wavelength range	2.325–4.250 µm
Spectral bandwidth (FWHM)	< 22 cm^{-1}
Acceptance aperture in plane of diffraction	> 10 mm
Acceptance aperture perpendicular to plane of diffraction	> 4 mm
Acceptance angle in plane of diffraction	±2°
Acceptance angle perpendicular to plane of diffraction	±3°
Diffraction angle	4.6°
RF frequency range	13.5–25 MHz

Table 5. SOIR echelle grating characteristics.

Wavelength range	2.2–4.3 µm
Diffraction orders	100–200
Steep edge angle = blaze angle	63.43° = arctan(2)
Number of grooves per mm	4
Groove spacing	250 µm
Total number of grooves	568
Ruled area	142 x 56 mm
Blank dimensions	150 x 60 x 25 mm
Blank material	Aluminium 6061-T6
Coating material	Au

Table 6. SOIR integrated detector cooler characteristics.

IR detector material	HgCdTe
Covered IR wavelength range	1.66–4.4 µm (FWHM)
Operating temperature	< 110K
Pixel configuration	2-D array organised as 320 columns by 256 rows programmable windowing
Pixel size	30 x 30 µm
Output level	1.6 (no light) to 4.4 V (full well)
Linearity (typical)	±1% for 25–92% of full well ±2% for 10–98% of full well
Gain setting	0.7 pF or 2.1 pF integration capacitor
Responsitivity (measured over complete wavelength range)	typical 76 V/nW per pixel @ 20 ms integration time and gain setting 0.7 pF
Readout speed	1–6 MHz for single output
Integration time	Minimum 3 µs; acceptance tested at 20 ms
Detector mounting	In dewar with f/4 cold screen
Integrated microcooler model	K508, modified for space applications (RICOR, Israel)
Steady-state cooling power (beginning of life)	4.1 W typical @ 24 V supply voltage (in 20°C air)
Pre-cooling power (beginning of life)	9.4 W typical @ 24 V supply voltage (in 20°C air)

320 columns by 256 rows. The vacuum encapsulation made it possible to operate in the open air, with full cooling and no risk of water condensation, an important feature that simplified development and testing. The sensitive area of 9600 x 7680 µm has a fill factor greater than 90% and is composed of pixels of 30 x 30 µm. All pixels are connected by means of indium bumps to a CMOS Readout Integrated Circuit (ROIC) that forms a sandwich with the MCT array. The ROIC reads the charge from each MCT photovoltaic diode via direct injection and integrates it on the pixel input capacitor (selectable to 0.7 pF or 2.1 pF) during a programmable integration time. Then the charges are converted to voltages, which appear on the serial outputs multiplexed per row and then per column. Although the ROIC allows for different ways and speeds of detector read-out, for power, telemetry and simplicity reasons the detector read-out is limited to a programmable window of 8 lines of 320 pixels, selectable within the detector area, and this in the single output mode at a 1 MHz rate. The

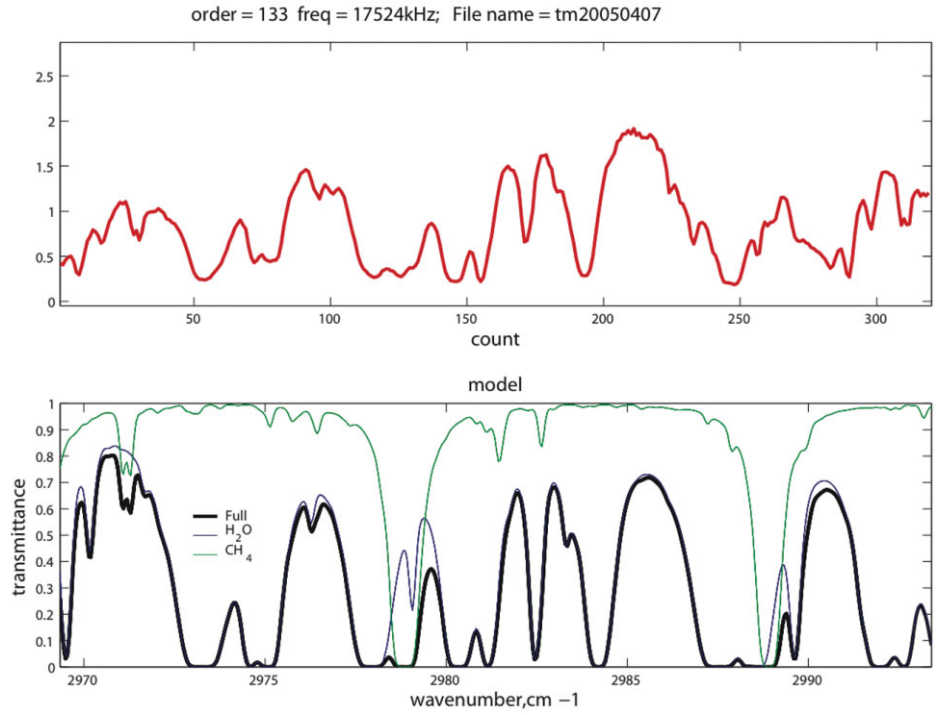

Fig. 39. Comparison of Earth atmosphere transmission model with SOIR data for order 133. Top: the blue curves xxx there are no blue curves!! xxx are 8 spectra obtained by applying 4-to-1 binning on 32 detector lines of 320 pixels each; the red is average of lines with maximal signal. Bottom: black is a model of Earth's atmosphere; green is CH_4 only; blue is H_2O only. Adopted resolving power for the synthetic spectra is 20000.

encapsulated detector is cooled by a Ricor Stirling-cycle mechanical cryocooler, as a part of the Sofradir integrated detector, allowing a detector temperature of 90K to be reached within a few minutes. The heat of SOIR is conducted to a side panel of Venus Express that is not normally illuminated by the Sun. The main characteristics of the customised version of the detector are given in Table 6.

SOIR underwent numerous tests, the most elaborate using the Sun as the source. The solar rays passing through the Earth's atmosphere were reflected by a mirror outside the laboratory and directed into SOIR in a cleanroom. Spectra corresponding to all orders of the echelle grating between 2.2 μm and 4.3 μm were recorded. A typical readout, spectrometer order 133, showing the features of atmospheric methane and H_2O, is shown in Fig. 39 and compared to a synthetic spectrum of the atmospheric transmission and solar spectrum. The water vapour absorption dominates, but the methane line at 2978 cm^{-1} is clearly seen, in a region where water vapour is not saturated. Such an instrument around Mars would certainly be useful for understanding the puzzling problem of methane.

4.3 SOIR and nightside, dayside and solar observations

When a solar occultation is programmed, Venus Express is oriented with the solar apertures of all three spectrometers towards the Sun. Solar spectra are recorded by SOIR, first above the atmosphere, then through it. Then, with the fixed orientation, the LOS of SOIR sees the nightside of Venus. The question then arises if SOIR sees the thermal emission from the ground and lower atmosphere. This would be very rich in information, since it crosses all altitudes. In fact, the difference in brightness at 3 μm between the solar disc and Venus ground at 700K is only a factor of 210. When looking at the Sun from the laboratory, the detector was saturated in 10 ms. In order to gain sensitivity, SOIR can be programmed with a 5 s integration time, and a large number of detector lines can be piled up numerically. The actual signal will depend crucially on the transparency of the cloud deck to radiation at 3 μm, which seems to be highly variable. If it works, it would open a very important route to studying the

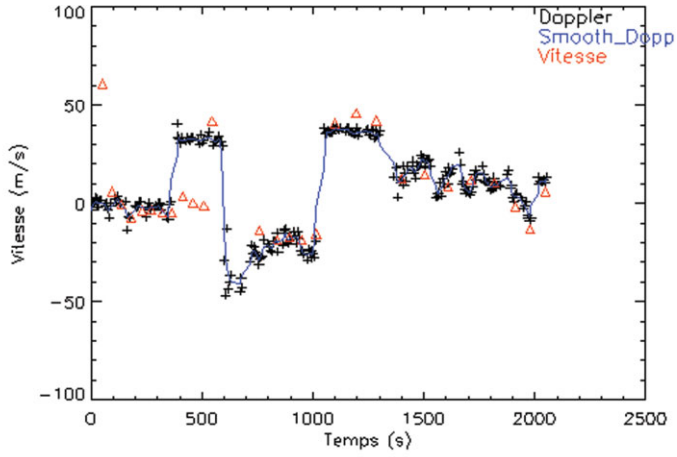

Fig. 40. Doppler shift measured in the reflected solar light at various points on the planet's disc (red triangles) at the Observatoire de Haute Provence using the Emilie spectrometer and the Astronomical Absolute Accelerometer (Bertaux et al., 2007). Black +: forward model assuming a solid rotation of the upper atmosphere at an equatorial velocity of 92 m/s.

lower atmosphere. Indeed, the spectral resolution of SOIR is 5–10 times the resolution of PFS, allowing the detection of HDO in the lower atmosphere (as was done from Earth), H_2O and possibly unforeseen minor constituents. Dayside measurements will also be attempted. The main exploration will be the spectral regions that escaped the measurements of Connes (1974) because of terrestrial absorption, at a spectral resolution which has never been achieved in space in this wavelength region. Even the solar spectrum recorded before the occultations will be a reference for future workers.

A second Flight Model of SOIR was prepared. It was used before launch and it will continue to contribute to ground testing. For example, the sensitivity limit will be measured.

5. Supporting Wind Measurements

The Venus winds will be measured by VMC, on the dayside by looking at the displacement of blue-UV markings. There is, however, the lingering problem of what is actually being measured. As on Earth, there may be waves of condensation that contribute to the appearance of the markings, so what is measured is not really a material displacement, but a phase motion. Indeed, some UV markings are actually locked in local time (around the sub-solar point), which proves the point.

Bertaux et al. (2007) have designed a method to measure the material displacement of the cloud particles, by recording the spectrum of the solar light scattered by the particles, and measuring the Doppler shift. It has been already proved with the Emilie spectrometer at the Observatoire de Haute Provence (F). This spectrometer is equipped with a high precision-calibration system, the Absolute Astronomical Accelerometer (invented by P. Connes). Winds of the order of 60–90 m/s have been recorded (Fig. 40), which is in line with the 4-day rotation (Gabsi et al., in preparation). A coordinated campaign is proposed for simultaneous observations from Venus Express and the ground, to disentangle the material motion of the particles from the wave phase motion.

References

Acuña, M.H., **xxxfull authors requiredxxx** (2001). Magnetic Field of Mars: Summary of Results from the Aerobraking and Mapping Orbits. *J. Geophys. Res.* **106**, 23403–23417.

Allen, D.A. & Crawford, J.W. (1984). Cloud Structure on the Dark Side of Venus. *Nature* **307**, 222–224.

Baines, K.V. **xxxfull authors requiredxxx** (2000). Detection of Sub-micron Radiation from the Surface of Venus by Cassini VIMS. *Icarus* **148**, 307–311.

Barth, C.A, Pearce, J.B., Kelly, K.K., Wallace, L. & Fastie, W.G. (1968). **xxx title xxxxx** *Science* **158**, 1675–**xxxx**.

Barth, C.A., Hord, C.W., Stewart, A.I., Lane, A.L., Duck, M.L. & Anderson, G.P. (1973). **xxxp11=1971xxx** Mariner 9 Ultraviolet Spectrometer Experiment: Seasonal Variation of Ozone on Mars. *Science* **179**, 795–796.

Barth, C.A., Hord, C.W., Pearce, J.B., Kelly, K.K., Anderson, G.P. & Stewart, A.I. (1971). Mariner 6 and 7 Ultraviolet Spectrometer Experiment: Upper Atmosphere Data. *J. Geophys. Res.* **76**, 2213–2227.

Barth, C.A., Stewart, A.I.F., Bougher, S.W., Hunten, D.M., Bauer, S.J. & Nagy, A.F. (1992). Aeronomy of the Current Martian Atmosphere. In *Mars* (Eds. **xxinitial?xx** Kieffer et al.), Univ. of Arizona Press, Tucson, Arizona, USA, pp **xxx page range of paper??xx**.

Bertaux, J.L. & Clarke, J.T. (1989). Deuterium Content of the Venus Atmosphere. *Nature* **338**, 567–568.

Bertaux, J.L., Leblanc, F., Perrier, S., Quémerais, E., Korablev, O., Dimarellis, E., Reberac, A., Forget, F., Simon, P.C., Stern, A.S. & Sandel, B.R. and the SPICAM Team (2005b). First Observation of Nightglow in the Upper Atmosphere of Mars: the NO bands in UV and Implications for Atmospheric Transport. *Science* **307**, 566–**xxx**. **xxxx ref not used in text xxx**

Bertaux, J.L., Blamont, J.E., Marcelin, M., Kurt, V.G. & Smirnov, A.S. (1979). Consequences of the Day-to-Night Variation of the Venus Exospheric Temperature. *Nature* **277**, 546–548.

Bertaux, J.L., Lépine, V.M., Kurt, V.G. & Smirnov, A.S. (1982). Altitude Profile of H in the Atmosphere of Venus from Lyman-alpha Observations of Venera 11 and Venera 12 and Origin of the Hot Exospheric Component. *Icarus* **52**, 221–224.

Bertaux, J.L. & Montmessin, F. (2001). **xxxp14=2000xxx**Isotopic Fractionation through Water Vapor Condensation: the Deuteropause, a Cold Trap for Deuterium in the Atmosphere of Mars. *J. Geophys. Res. Planets* **106** E12, 32879–32884.

Bertaux, J.L., Fonteyn, D., Korablev, O., Chassefière, E., Dimarellis, E., Dubois, J.P., Hauchecorne, A., Cabane, M., Ranou, P., Levasseur-Regourd, A.C., Cernogora, G., Quemerais, E., Hermans, C., Kockarts, G., Lippens, C., De Maziere, M., Moreau, D., Muller, C., Neefs, E., Simon, P.C., Forget, F., Hourdin, F., Talagrand, O., Moroz, V.I., Rodin, A., Sandel, B. & Stern, A. (2000). The Study of the Martian Atmosphere from Top to Bottom with SPICAM Light on Mars Express. *Planet. Space Sci.* **48**, 1303–1320.**xxxx ref not used in text xxx**

Bertaux, J.L., Blamont, J.E., Lépine, V.M., Kurt, V.G., Romanova, N.N. & Smirnov, A.S. (1981). Venera 11 and Venera 12 Observations of EUV Emissions from the Upper Atmosphere of Venus. *Planet. Space Sci.* **29**, 149–166.

Bertaux, J.L., Leblanc, F., Witasse, O., Quémerais, E., Lilensten, J., Stern, S.A., Sandel, B. & Korablev, O. (2005). Discovery of Aurora on Mars. *Nature* **435**, 790–794.

Bertaux, J.L., Widemann, T., Hauchecorne, A., Moroz, V.I. & Ekonomov, A.P. (1996). Vega-1 and Vega-2 Entry Probes: an Investigation of Local UV Absorption (220–400 nm) in the Atmosphere of Venus (SO_2, Aerosols, Cloud Structure), *J. Geophys. Res.* **101**, 12709–12745.

Bertaux, J.L., Korablev, O., Perrier, S., Quémerais, E., Montmessin, F., Leblanc, F., Lebonnois, S., Lefèvre, F., Forget, F., Fedorova, A., Rannou, P., Dimarellis, E., Reberac, A., Fonteyn, D., Chaufray, J.Y., Guibert, S. and the SPICAM Team (2006). SPICAM on Mars Express: Observing Modes and Overview of UV Spectrometer Data and Scientific Results. *J. Geophys. Res.*; in press. **xxx if (2006), must be published by now xxx**

Bertaux, J.L. (2007). **xxxx missing ; used on p35xxxx**

Bougher, S.W., Gerard, J.C., Stewart, A.I.F. & Fesen, C.G. (1990). **xxxxx title required xxxxx** *J. Geophys. Res.* **95**, 6271–6284.
Bougher, S.W., Alexander, M.J. & Mayr, H.G. (1997). **xxxxx title required xxxxx** In *Venus II* (Eds. S.W. Bougher, D.M. Hunten & R.J. Phillips), The University of Arizona Press, Tucson, Arizona, USA, pp **xxx page range of article required xxx xxxx ref not used in text xxx**
Bougher, S.W., Roble, R.G., Ridley, E.C. & Dickinson, R.E. (1990). The Mars Thermosphere. II. General Circulation with Coupled Dynamics and Composition. *J. Geophys. Res.* **95**, 14811–14827.
Boyer, C. & Camichel, H. (1965). Étude Photographique de la Rotation de Vénus. *C.R. Acad. Sci., Paris* **260**, 809–810.
Cheng, B.M., Chew, E.P., Ching-Ping Liu, Bahou, M., Yuan-Pern Lee, Yuk L. Yung & Gerstell, M.F. (1999). Photo-Induced Fractionation of Water Isotopomers in the Martian Atmosphere. *Geophys. Res. Letters* **26**, 3657–3660.
De Bergh, C., Bezard, B., Owen, T., Crisp, D., Maillard, J.-P. & Lutz, B.L. (1991). Deuterium on Venus: Observations from Earth. *Science* **251**, 547–549.

connes 1974 missing, called out p35

Connes, P., Noxon, J.F., Traub, W.A. & Carleton, N.P. (1979). O_2 ($^1\Delta$) Emission in the Day and Night Airglow of Venus. *Astrophys J.* **233**, L29–L32.

donahue et al 1997 missing, called out p29

Donahue, T.M., Hoffman, J.H., Hodges, R.R. & Watson, A.J. (1982). Venus was Wet – A Measurement of the Ratio of Deuterium to Hydrogen. *Science* **216**, 630–633.
Donahue, T.M. (1999). New Analysis of Hydrogen and Deuterium Escape from Venus. *Icarus* **141**, 226–235.
Esposito, L.W, Bertaux, J.L., Krasnopolsky, V. Moroz, V.I. & Zasova, L.L. (1997). Chemistry of Lower Atmosphere and Clouds. In *Venus II* (Eds. S.W. Bougher, D.M. Hunten & R.J. Phillips), The University of Arizona Press, Tucson, Arizona, USA, pp415–458. **xxxx ref not used in text xxx**
Esposito, L.W. (1984). Sulfur Dioxide: Episodic Injection Shows Evidence for Active Venus Volcanism. *Science* **223**, 1072–1074.
Fegley, B., Zolotov, M.Y. & Lodders, K. (1997). The Oxidation State of the Lower Atmosphere and Surface of Venus. *Icarus* **125**, 416–439.
Feldman, P.D., Moos, H.W., Clarke, J.T. & Lane, A.L. (1979). **xxx title required xxx** *Nature* **279**, 221–**xxx**.

forget et al 2006 missing, called our p17

Fox, J.L. (1986). Models for Aurora and Airglow Emissions from Other Planetary Atmospheres. *Can. J. Phys.* **64**, 1631–1656.

fox et al 1991 missing, called out p9

Fox, J.L. (1992). Airglow and Aurora in the Atmospheres of Venus and Mars. In *Venus and Mars: Atmospheres, Ionospheres, and Solar Wind Interactions* (Eds. J. G. Luhmann, M. Tatrallyay & R.O. Pepin), AGU Geophys. Monogr. 66, Washington, DC, USA, 191–221.
Gabsi, Y., Bertaux, J.L., Schmitt, J., Guibert, S. & Hauchecorne, A. (2006). Measurements of Wind Velocity on Venus with Absolute Accelerometry. **xxx publication details xxxx**
Glenar, D.A., Hillman, J.J., Saiff, B. & Bergstralh, J. (1994). Acousto-optic Imaging Spectropolarimery for Remote Sensing. *Appl. Opt.* **33**(31),

7412–7424.
Gurwell, M.A. (1995). Evolution of Deuterium on Venus. *Nature* **378**, 22–23.
Keating, G.M. **xxx other authors required xxx** (1985). **xxx paper title required xxx** In *The Venus International Reference Atmosphere* (Eds A.J. Kliore, V.I. Moroz & G.M. Keating), **xxxpublisher details xxx** , pp117–171.

korablev and bertaux 2003 missing, called out p17

Korablev, O.I., Bertaux, J.-L. & Dubois, J.-P. (2001). Occultation of Stars in the UV: Study of the Atmosphere of Mars. *J. Geophys. Res.* **106**(E4), 7597–7610.
Korablev, O., Bertaux, J.-L., Grigoriev, A., Dimarellis, E., Kalinnikov, Yu., Rodin, A., Muller, C. & Fonteyn, D. (2002b). An AOTF-based Spectrometer for the Studies of Mars Atmosphere for Mars Express ESA mission. *Adv. Space Res.* **29**:2, 143–150.
Korablev, O.I., Bertaux, J.L., Dimarellis, E., Grigoriev, A., Kalinnikov, Yu., Stepanov, A. & Guibert, S. (2002c). AOTF-based Spectrometer for Mars Atmosphere Sounding. *Proc. SPIE* **4818**, 261–271.
Korablev, O.I., Bertaux, J.-L. & Vinogradov, I.I. (2002a). Compact High-resolution IR Spectrometer for Atmospheric Studies. *Proc. SPIE* **4818**, 272–281.
Korablev, O.I., Bertaux, J.-L., Vinogradov, I.I., Kalinnikov, Yu.K., Nevejans, D. & Neefs, E. (2004). Compact High-resolution Echelle-AOTF NIR Spectrometer to Study the Details of Planetary Atmospheres. In *Mars Express: The Scientific Payload* (Ed. A. Wilson), SP-554, ESA Publications Division, European Space Agency, ESTEC, Noordwijk, The Netherlands, pp73–80.
Krasnopolsky, V.A., Mumma, M.J. & Gladstone, G.R. (1998). Detection of Atomic Deuterium in the Upper Atmosphere of Mars. *Science* **280**, 1576–1580.
Kurucz, R. (1995). The Solar Spectrum: Atlases and Line Identifications. *Workshop on Laboratory and Astronomical High Resolution Spectra, ASP Conference Series* **81**, ASP, San Francisco, USA, pp17–**XX**.
Leblanc F., Chaufray, J.Y., Lilensten, J., Witasse, O., Bertaux, J.L and the SPICAM Team (2006). The Martian Dayglow as seen by SPICAM UV Spectrometer on Mars Express. *J. Geophys. Rev.*, in press **xxxmust be published by now xxx**
Lebonnois S., Quémerais, E., Montmessin, F., Lefèvre, F., Perrier, S., Bertaux, J.L. & Forget, F. (2006). Vertical Distribution of Ozone on Mars as Measured by SPICAM/Mars Express using Stellar Occultations. *J. Geophys. Rev.*, in press **xxx must be published by now if 2006 xxx**

montmessin et al 2006a + 2006b missing, called out p18

Montmessin, F., Quémerais, E., Bertaux, J.L., Korablev, O., Fedorova, A., Rannou, P. & Lebonnois, S. (2006). Stellar Occultations at UV Wavelengths by the SPICAM Instrument: Retrieval and Analysis of Martian Haze Profiles. *J. Geophys. Rev.*, in press. **xxx must be published by now if 2006 xxx**
Nevejans, D., Neefs, E., Van Ransbeeck, E., Berkenbosch, S., Clairquin, R., De Vos, L., Moelans, W., Glorieux, S., Baeke, A., Korablev, O., Vinogradov, I., Bach, B., Dubois, J.P. & Villard, E. (2006). Compact High-resolution Space-borne Echelle Grating Spectrometer with AOTF-based Order Sorting for the Infrared Domain from 2.2 to 4.3 micrometer. *Applied Optics*, in press. **xxx must be published by now if 2006 xxx**
xxx initials required for author names Paxton & Anderson. (1992). **xxx title required xxx** In *Venus and Mars: Atmospheres, Ionospheres, and Solar Wind Interactions* (Eds. J.G. Luhmann, M. Tatrallyay & R.O. Pepin), AGU

Geophys. Monogr. 66; Washington, DC, USA, pp191–xxx.
Perrier, S., Bertaux, J.L., Lefèvre, F., Lebonnois, S., Korablev, O., Fedorova, A. & Montmessin, F. (2006). Global Climatology of Ozone on Mars from SPICAM/MEX UV Measurements. *J. Geophys. Rev.*, in press. **xxx must be published by now if 2006 xxx**
Philips, J.L., Stewart, A.I.F. & Luhmann, J.G. (1986). The Venus Ultraviolet Aurora: Observations at 130.4 nm. *Geophys. Res. Letters* **13**, 1047–1050.
Quémerais, E., Bertaux, J.L., Korablev, O., Dimarellis, E., Cot, C., Sandel, B.R. & Fussen, D. (2006). Stellar Occultations Observed by SPICAM on Mars Express. *J. Geophys. Rev.*, in press. **xxx must be published by now if 2006 xxx**
Rannou, P., Bertaux, J.L., Perrier, S., Montmessin, F. & Reberac, A. (2006). Dust and Cloud Detection at Mars Limb from UV Scattered Sunlight with SPICAM. *J. Geophys. Rev.*, in press. **xxx must be published by now if 2006 xxx**
Roscoe, H.K., Freshwater, R.A., Wolfenden, R., Jones, R.L., Fish, D.J., Harries, J.E. & Oldham, D.J. (1994). Using Stars for Remote Sensing of the Earth's Stratosphere. *Appl. Optics* **33**, 7126–7131.
Santer, R., Deschamps, M., Ksanfomaliti, L.V. & Dollfus, A. (1985). Photo-polarimetric Analysis of the Martian Atmosphere by the Soviet Mars-5 Orbiter. I - White Clouds and Dust Veils. *Astron. Astroph.* **150**(2), 217–228.
Smith, G.R. & Hunten, D.M. (1990). Study of Planetary Atmospheres by Absorptive Occultations. *Rev. of Geophys.* **28**, 117–xxx.
Stewart, A.I.F. & Barth, C.A. (1979). **xx title required xxx** *Science* **205**, 59–xxx.
Stewart, A.I., Barth, C.A. & Hord, C.W. (1972). Mariner 9 Ultraviolet Spectrometer Experiment: Structure of Mars' Upper Atmosphere. *Icarus* **17**, 469–474.
Stewart, A.I.F., Anderson, Jr., D.E., Esposito, L.W. & Barth, C.A. (1979). **xxx title required xxx** *Science* **203**, 777–XXX.
Stewart, A.I.F. **xxx other authors required xxx** (1980). **xxx title required xxx** *J. Geophys. Res.* **85**, 7861–7870.

Acknowledgements.
The authors express their gratitude to all those at ESA who participated in the preparation of this mission: H. Svedhem as Project Scientist, and O. Witasse as his deputy, H. Eggel for his constant technical dedication, D. McCoy as Project Manager, and R. Hoofs for the development of operations software. We acknowledge the important role of D. Titov, for putting together contradictory requirements from the various PIs. We thank EADS Astrium for the design and construction of the spacecraft, and in particular A. Clochet for the payload. We thank our collaborators at the three institutes for the design and fabrication of the instrument (Service d'Aéronomie, BIRA and IKI), including the important help of J.-L. Maria and M. Meftah at Service d'Aéronomie. We thank CNRS and CNES for financing SPICAM in France, the Russian Academy of Sciences for support at IKI, and NASA for support of US Co-Investigators. We express our gratitude for the financial support from the Belgian Federal Science Policy Office, who completely funded the design and manufacturing of SOIR and part of the construction of SPICAM on Mars Express (ESA PRODEX contract 90113) during 2003–2005. We thank F. Rocard at CNES and M. Lalaurie at Centre Spatial de Toulouse (CNES) for his support in difficult circumstances. Finally, we acknowledge the excellent work of Sofradir, which developed a custom-designed mechanically-cooled detector of very high performance in a short time and on schedule, and its Chairman, M. Bensousan.